Scilight

*Nano-electrochemistry & Nano-photochemistry*

https://www.sciltp.com/journals/nenp

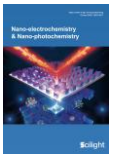

*Review*

# Graphene Quantum Dots: Synthesis, Properties, and Applications in Electroanalysis

Yuqian Geng [1], Yue Cao [2] and Junjie Zhu [1,*]

[1] State Key Laboratory of Analytical Chemistry for Life Science, School of Chemistry and Chemical Engineering, Nanjing University, Nanjing 210023, China

[2] State Key Laboratory of Flexible Electronics (LoFE) and Institute of Advanced Materials (IAM), Nanjing University of Posts and Telecommunications, Nanjing 210023, China

* Correspondence: jjzhu@nju.edu.cn

**How To Cite:** Geng, Y.; Cao, Y.; Zhu, J. Graphene Quantum Dots: Synthesis, Properties, and Applications in Electroanalysis. *Nano-electrochemistry & Nano-photochemistry* **2025**, *1*(1), 3. https://doi.org/10.53941/nenp.2025.100003.

Received: 9 July 2025
Revised: 31 October 2025
Accepted: 6 November 2025
Published: 13 November 2025

**Abstract:** Graphene quantum dots (GQDs) are zero-dimensional carbon nanomaterials that integrate the π-conjugated structure of graphene with size-dependent and quantum-confined optical properties. Owing to their tunable electronic band gaps, excellent electrical conductivity, chemical versatility, and good biocompatibility, GQDs have emerged as promising materials for electroanalytical applications. This review summarizes recent advances in the synthesis, properties, modifications, and electroanalytical applications of GQDs, with an emphasis on the structure–function relationships of GQDs in electrochemical, electrochemiluminescence (ECL), and photoelectrochemical (PEC) sensing systems, thereby providing useful insights into future research directions in this field.

**Keywords:** graphene quantum dots; electroanalysis; carbon nanomaterial

## 1. Introduction

In 2004, Novoselov et al. successfully isolated two-dimensional (2D) graphene nanosheets from bulk graphite using the adhesive tape method. Since then, graphene has gained recognition for its exceptional mechanical strength, low density, excellent electrical conductivity, and outstanding chemical stability. However, the perfectly ordered hexagonal honeycomb lattice of graphene exhibits limited chemical reactivity due to the absence of active reaction sites. Additionally, strong π-π interactions and van der Waals forces cause graphene sheets to aggregate, thereby hindering their dispersion in conventional solvents.

In 2008, graphene quantum dots (GQDs) were first fabricated via oxygen plasma etching [1]. Subsequent studies have revealed the size-dependent optical and electronic properties of GQDs and their broad applications in energy storage [1], catalysis [2,3], biomedicine [4], and sensing [5−7]. Although termed quantum dots, it has been stated that, unlike conventional semiconductor quantum dots, the fluorescence emission mechanisms of GQDs are more complex, often involving surface trap states associated with functional groups and structural defects [7]. As a specific subtype of carbon dots, GQDs are characterized by their π-conjugated framework, quantum confinement effects, and crystalline graphitic domains. These features differentiate GQDs from other carbon dots, such as carbon quantum dots (CQDs), which have a spherical crystalline structure, and carbon nanodots (CNDs), which possess an amorphous structure lacking evident quantum confinement.

GQDs are nanoscale graphene fragments consisting of single or a few atomic layers, typically terminated with various edge functional groups. The hexagonal lattice structure inherited from graphene provides excellent electrical conductivity, while quantum confinement and surface states govern their photoluminescence (PL) behavior. Additionally, the presence of surface functional groups, intrinsic defects, and heteroatom dopants enhances the chemical reactivity of GQDs. These features make GQDs highly suitable for electroanalysis. First,

GQDs facilitate efficient charge transfer and transport at interfaces [8−10]. Second, their high chemical reactivity enables effective electrocatalysis under an applied potential [11−13]. Third, the large specific surface area allows GQDs to form strong interactions or composites with other nanomaterials, which is crucial for signal amplification [8,11,14−16]. Finally, the unique electronic band structure of GQDs underpins their applications in electrochemiluminescence (ECL) and photoelectrochemical (PEC) sensing [17−21].

Recent reviews have comprehensively summarized the synthesis, properties, and applications of GQDs [22,23]. However, a systematic and focused evaluation of their roles in electroanalysis remains scarce. Although previous reviews have addressed electrochemical sensing applications of GQDs, most have concentrated on specific analytes or device architectures, leaving the multifunctional electrochemical behaviors of GQDs insufficiently integrated [24,25]. This review provides an in-depth analysis of the fundamental mechanisms by which GQDs enhance electroanalytical performance. We present a comprehensive overview of recent progress in the synthesis strategies, physicochemical properties, and electroanalytical applications of GQDs. A comprehensive overview of recent progress in the synthesis strategies, physicochemical properties, and electroanalytical applications of GQDs is presented in this review. By establishing a function-oriented analytical framework, we aim to elucidate the underlying structure-property-function correlations that connect GQD properties to their electroanalytical applications. This approach provides a mechanistic and principle-guided understanding, thereby facilitating the rational design of GQD-based sensing platforms for environmental monitoring, food safety, biosensing, and related applications.

## 2. Synthesis and Purification

The synthetic route has been demonstrated to strongly influence not only the production cost, reaction time, and operating conditions, but also the size, structural uniformity, and surface functionalization of the resulting GQDs. Synthesis strategies are generally classified into top-down and bottom-up approaches. In top-down approaches, bulk carbon materials such as graphene [26,27], graphene oxide (GO) [28−30], coke [31], and coal [32] are broken down into nanoscale fragments. Although top-down approaches utilize low-cost precursors, they often suffer from low product yields. In contrast, bottom-up methods involve the carbonization or condensation of small molecular precursors, such as substituted benzene derivatives [33], glucose [34], and citric acid [35], leading to the controlled formation of $sp^2$-hybridized carbon frameworks. The products from bottom-up methods typically exhibit higher yields and facilitate heteroatom doping. However, these methods often require precise control over multi-step reactions, which limits large-scale production. It is worth noting that post-synthetic purification is essential to achieve uniform particle size and optimal performance of GQDs. Common purification techniques include dialysis [36], salting-out extraction [37], solid-phase extraction (SPE) [38], and so forth.

### *2.1. Bottom-up Approaches*

#### 2.1.1. Hydrothermal and Pyrolysis Synthesis

As the reaction temperature rises, a series of chemical transformations occur, including dehydration, condensation, nucleation, growth, and eventual carbonization into GQDs, as illustrated in Figure 1A [34]. The morphology and elemental composition of the resulting products are influenced by multiple factors, including reaction temperature, heating duration, solvent type, and precursor concentration. The heating process may be conducted in a solvent medium (hydrothermal synthesis) or under an inert atmosphere (pyrolytic synthesis). In hydrothermal synthesis, intermolecular condensation reactions occur between precursors, and dehydration promotes the formation of $sp^2$-hybridized carbon networks. For instance, Guo et al. prepared GQDs bearing hydroxyl and amino functional groups from 1,5-dinitronaphthalene in an aqueous ammonium solution at 200 °C for 18 h [39]. Pyrolysis synthesis, another widely used bottom-up method, typically requires higher reaction temperatures under inert conditions to achieve carbonization. For example, Martins et al. synthesized nitrogen- and sulfur-co-doped GQDs (N,S-GQDs) from citric acid and L-cysteine by heating the mixture to 240 °C [40]. However, both conventional hydrothermal and pyrolytic methods are relatively time-consuming. Microwave-assisted synthesis has been proposed as an effective strategy to shorten GQD growth times to only 5–10 min [41]. This technique has been shown to significantly accelerate synthesis and enhance quantum yield by precisely controlling temperature and pressure during synthesis [41] or subsequent post-treatment processes [42].

#### 2.1.2. Soft-Template Method

The soft-template method offers nano-reactors for the controlled synthesis of GQDs with a narrow size distribution, thereby minimizing or eliminating the need for post-synthetic purification. Li et al. synthesized single-layer N-doped GQDs (N-GQDs) using 1,3,5-triamino-2,4,6-trinitrobenzene (TATB) as both the template and

precursor [43]. The symmetrical intermolecular carbonization of TATB, enabled by its planar aromatic framework and six nitrogen-containing functional groups, facilitated the formation of small and uniform GQDs (2–5 nm) with high nitrogen incorporation. Furthermore, the gas evolution during TATB pyrolysis expanded interlayer spacing, thereby promoting N-GQD formation. In another study, Tang et al. employed polyethylene micelles as a soft template and glucose as the carbon precursor (Figure 1B) [44]. A limited number of glucose molecules were confined within each micelle, where they underwent uniform pyrolysis, nucleation, and growth under microwave-assisted hydrothermal conditions, yielding GQDs with diameters ranging from 1.5 to 3.9 nm.

### 2.1.3. Step-Wise Organic Synthesis

Several studies have reported the preparation of GQDs through well-controlled chemical reactions. Yan et al. developed a solution-based approach to produce stable colloidal GQDs [33]. As demonstrated in Figure 1C, the process begins with substituted benzene derivatives, such as 3-iodo-4-bromoaniline, and proceeds through a sequence of organic reactions, ultimately yielding GQDs with well-defined molecular structures.

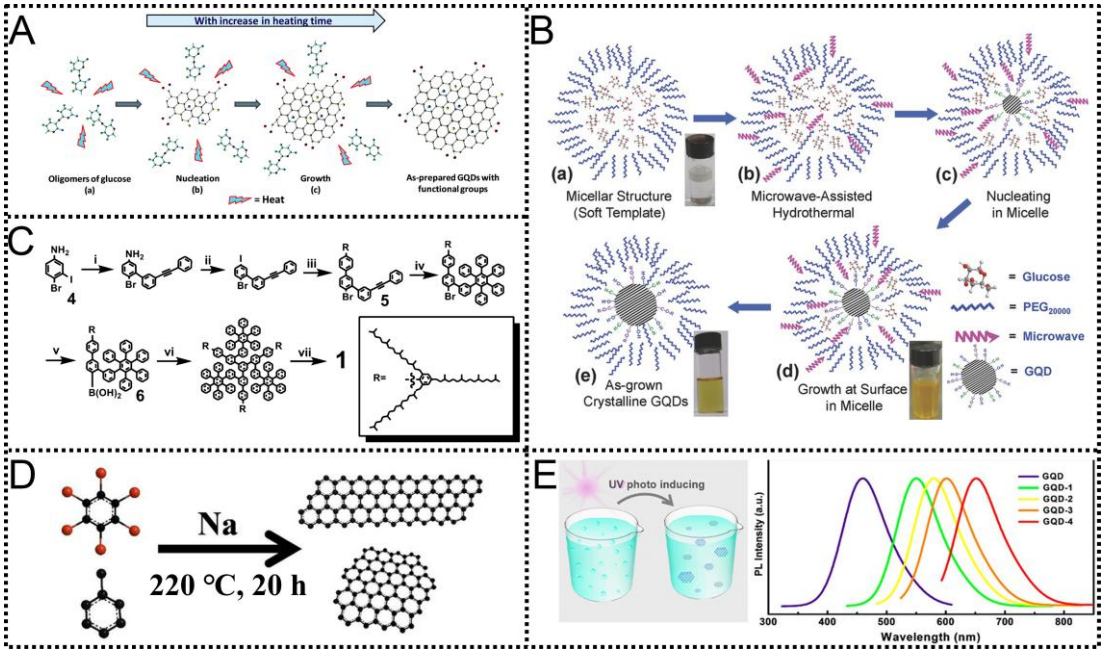


**Figure 1.** Schematic illustrations of representative bottom-up synthesis routes for GQDs from various small molecules. (**A**) Hydrothermal/pyrolysis synthesis from glucose precursors. Reproduced with permission [34]. Copyright 2016, The Royal Society of Chemistry. (**B**) Soft-template synthesis using polyethylene micelles and glucose. Reproduced with permission [44]. Copyright 2013, WILEY-VCH. (**C**) Step-wise organic synthesis from substituted benzene derivatives. Reproduced with permission [33]. Copyright 2010, American Chemical Society. (**D**) Metal-reduction synthesis of GQDs on graphene nanoribbons. Reproduced with permission [45]. Copyright 2015, American Chemical Society. (**E**) Ultraviolet irradiation-induced free radical polymerization for GQD synthesis. Reproduced with permission [46]. Copyright 2017, American Chemical Society.

### 2.1.4. Others

Another bottom-up method involves synthesizing GQDs through precursor reduction in the presence of metals. Jin et al. prepared GQDs supported on graphene nanoribbons, which were subsequently utilized as effective catalysts for the oxygen reduction reaction (ORR) [45]. As demonstrated in Figure 1D, the reaction was conducted at 220 °C for 20 h, using methylbenzene and hexabromobenzene as precursors and sodium as the reductant. Furthermore, Zhu et al. developed a mild, environmentally friendly, and versatile method for GQD synthesis and heteroatom doping via free-radical polymerization under ultraviolet irradiation [46]. In their study, an aqueous solution of salicylic acid was used as the precursor and exposed to ultraviolet light for 2 h. As shown in Figure 1E, ultraviolet irradiation generated free radicals from the solvent molecules, which were rapidly captured by salicylic acid, forming secondary aromatic radicals that subsequently reorganized into GQDs. By adjusting the precursor concentration, both the size and emission wavelength of GQDs could be precisely controlled. This approach achieved an exceptionally high yield of 86%, owing to its mild reaction conditions.

### *2.2. Top-down Approaches*

#### 2.2.1. Hydrothermal Cleavage

In this method, a range of chemicals, including strong acids, free radicals, and bases, are utilized to exfoliate GQDs from bulk graphene-like precursors, particularly under the synergistic effect of elevated temperature. In addition to conventional carbon-based materials, such as graphene and GO, biomass-derived precursors represent a promising yet underutilized source for GQD synthesis [47].

Concentrated strong acids are frequently utilized as oxidants in hydrothermal cleavage reactions, introducing defects such as epoxy groups into the carbon lattice, which serve as active sites for subsequent chemical reactions. GQDs produced by this method typically contain oxygenated functional groups, which can be removed through reduction using appropriate reductive agents [48]. Vazquez-Nakagawa et al. demonstrated the acid-assisted hydrothermal cleavage of GO [28−30]. In their study, GO was oxidized in a mixture of sulfuric and nitric acids at 120 °C for 48 h, followed by neutralization and dialysis to yield water-soluble GQDs. Despite the simplicity of the hydrothermal oxidation cleavage method, the use of strong acids is highly corrosive and challenging to completely remove.

Free radical initiators, such as $KO_2$ [29], $H_2O_2$ [49], and oxone [50], enable oxidation cleavage in the absence of strong acids. The process involves radical generation, oxidation, and solvothermal reduction to cleave C–C bonds. For example, Zhao et al. reported the hydrothermal synthesis of GQDs from GO using KO2, in which a mixture of GO and $KO_2$ was heated in deionized water at 200 °C for 24 h, as depicted in Figure 2A [29]. Compared to strong acids, free radical reagents offer a more environmentally friendly alternative.

Additionally, alkaline reagents have been employed in hydrothermal cleavage for GQD production. For instance, a method for preparing amino-functionalized GQDs (af-GQDs) using ammonia has been reported [51]. In this procedure, oxidized graphene sheets and ammonia were heated at 70–150 °C for 5 h. This thermal treatment induced the cleavage of $sp^2$ domains through nucleophilic substitution by ammonia. The degree of amino functionalization can be modulated by adjusting ammonia concentration and reaction temperature. Although this method operates at relatively mild temperatures, similar to other hydrothermal cleavage techniques, it still requires extended heating durations.

#### 2.2.2. Physical Cleavage

Lasers with specific wavelengths have also been employed to synthesize GQDs via physical cleavage. Instantaneous laser irradiation induces photothermal vaporization [52] or ablation [53] of precursors, followed by recrystallization or retention of GQDs. For example, Kang et al. reported the rapid fabrication of GQDs from multi-walled carbon nanotubes (MWCNTs) using pulsed laser ablation in liquid (PLAL) [53], as shown in Figure 2B. MWCNTs were ablated by lasers with wavelengths of 355 nm and 532 nm respectively. Following a 10-min ablation, the 532-nm laser produced GQDs, while the 355-nm laser, with higher photon energy, led to solvent (ethanol) decomposition and introduced additional oxygen-containing functional groups into the products. These results suggest that edge functionalization can be controlled by adjusting the laser wavelength. The properties of GQDs can also be affected by laser output power, scan speed, and choice of solvent. Ultrasonic waves, which generate alternating high and low pressures in liquids, causing the formation and collapse of small vacuum bubbles, have also been used as a physical driving force for GQD synthesis. The resulting high-energy environment promotes C–C bond cleavage and precursor dissociation [32,54]. Zhang et al. prepared GQDs from coal using ultrasonication. As shown in Figure 2C [32], the precursor dispersed in dimethyl formamide (DMF) was subjected to ultrasonication for 2 h. After purification, the obtained GQDs exhibited a quantum yield of 5.98%. Physical cleavage offers an attractive alternative by avoiding high temperatures and corrosive acids, rendering it well-suited for large-scale GQD production. Nevertheless, the main limitation of laser irradiation lies in the substantial cost of the required equipment. In contrast, ultrasonication is more cost-effective, but generally yields GQDs with fewer defects and functional groups, which may limit their chemical reactivity.

#### 2.2.3. Electrochemical Method

Radicals generated by oxidizing solvent molecules under an applied potential facilitate the cleavage of C–C bonds in precursors. Electrolyte ions subsequently intercalate into graphene layers under the electric field, creating active sites that promote the formation of nanoscale GQDs [27]. Kalita et al. demonstrated the electrochemical synthesis of GQDs for use in a soil moisture sensor [30]. As shown in Figure 2D, GO was drop-cast onto the glassy carbon electrode (GCE) to serve as the working electrode. Applying an anodic potential of 1.05 V induces oxidation of GO, followed by reduction at −1.05 V to produce size-controlled GQDs. The morphology and size of

GQDs can be tuned by adjusting the oxidation/reduction time, applied potential, and electrolyte concentration. The electrochemical method provides a straightforward strategy for producing uniform GQDs without the need for elevated temperatures. Further investigation into the relationship between operational parameters and product properties is essential for advancing green chemical synthesis.

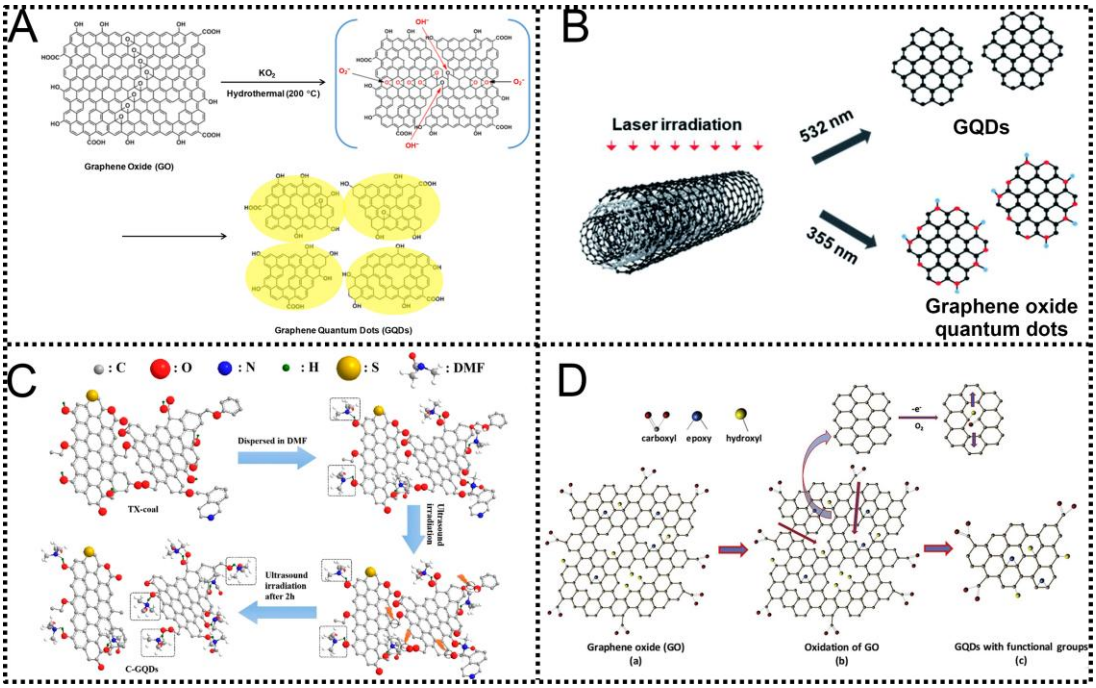


**Figure 2.** Schematic illustrations of top-down fabrication strategies for GQDs from various carbon precursors. (**A**) Hydrothermal cleavage of graphene oxide using $KO_2$ as a radical initiator. Reproduced with permission [29]. Copyright 2017, Elsevier. (**B**) Laser irradiation-based ablation of multi-walled carbon nanotubes for GQD production. Reproduced with permission [53]. Copyright 2019, The Royal Society of Chemistry. (**C**) Ultrasonication-assisted exfoliation of coal into GQDs. Reproduced with permission [32]. Copyright 2019, American Chemical Society. (**D**) Electrochemical synthesis of GQDs via potential-induced oxidation and reduction of GO. Reproduced with permission [30]. Copyright 2020, Elsevier.

Although bottom-up methods often produce GQDs with enhanced crystallinity and controlled heteroatom doping, beneficial for electrical conductivity and the formation of catalytic sites, they may also generate small molecular fluorophores, which can complicate the interpretation of electrochemical and optical signals. In contrast, top-down approaches generally yield GQDs with more well-defined graphene lattices; however, they may also exhibit broader size distributions and insufficient functionalization, potentially limiting their electrocatalytic activity. Consequently, the choice of synthesis method is not merely a trade-off between cost and yield but represents a critical factor in determining the electrochemical performance of the resulting GQDs.

### *2.3. Purification*

Purification is essential to ensure accurate reporting of GQD properties. GQD synthesis, particularly through bottom-up approaches, often produces a mixture of target nanoparticles, unreacted precursors, and various molecular by-products. These by-products, including residual molecular fluorophores and chiral precursors, can interfere with the observed PL or chiroptical properties, potentially leading to misinterpretation of the intrinsic characteristics of GQD [55−57].

A variety of purification techniques are available, with the choice determined by the solubility and size of the target products and by-products. Dialysis, a common method for purifying water-soluble GQDs, employs membranes with specific molecular weight cut-offs. However, this method is not universally applicable, particularly when by-products are hydrophobic or poorly soluble in water. In such cases, prolonged dialysis or alternative strategies, such as liquid-liquid extraction, may be required. More advanced techniques, such as size-exclusion chromatography (SEC) and high-performance liquid chromatography (HPLC), provide superior resolution for separating GQDs from smaller molecular impurities and even enable fractionation based on size [56,57]. Verification of purification efficacy is equally important. Conventional characterization techniques, such as transmission electron microscopy (TEM) and atomic force microscopy (AFM), are inadequate for distinguishing

GQDs from molecular aggregates with similar morphologies. Nuclear magnetic resonance (NMR) spectroscopy has proven indispensable in this context. According to Bartolomei et al., pure GQDs exhibit broad, unresolved signals in their NMR spectra, while sharp, well-defined peaks indicate the presence of residual small molecules [55].

In summary, although techniques such as dialysis, HPLC, and NMR have demonstrated effectiveness, their optimization for specific GQD materials remains essential. Furthermore, the lack of standardized purification and characterization protocols has led to poor reproducibility and challenges in evaluating GQD quality, including size distribution and surface chemistry. The following key unresolved issues remain: the scalable, eco-friendly production of high yields of pure, monodisperse GQDs; the development of consensus guidelines for GQD synthesis; and the enhancement of reliability in GQD-based research.

## 3. Properties and Regulations

Many studies have comprehensively reviewed the intrinsic properties, bandgap, and optical characteristics of GQDs, with the aim of understanding and precisely controlling their performance as semiconductors and photoluminescent emitters [3,58,59]. Moreover, the electroanalytical performance of GQDs has attracted growing attention. Therefore, this section focuses on reviewing key properties and regulation strategies related to the electroanalytical performance of GQDs.

### *3.1. Properties*

#### 3.1.1. Intrinsic Properties

GQDs primarily consist of carbon ($sp^2$ or $sp^3$ hybridized) and hydrogen atoms, both of which are abundant in living organisms. Consequently, their low cytotoxicity and high biocompatibility make GQDs suitable for both in vitro and in vivo biological studies [60]. However, oxidation is inevitable during synthesis, resulting in the presence of oxygen in most reported GQDs. This oxygen exists either as atomic doping or as functional groups. Furthermore, researchers have introduced various heteroatoms or functional groups to enhance GQD performance, incorporating trace amounts of nitrogen, phosphorus, sulfur, and other elements [13,61−63]. GQDs generally possess particle sizes ranging from 1 to 10 nm and feature a graphene lattice structure composed of one or a few graphene sheets. The edges or interlayer defects of graphene sheets contain diverse chemical moieties. Studies show that an increase in oxygen-containing groups at the edges shifts the X-ray diffraction peak from 23° to 22.1°, indicating a larger interlayer spacing [64]. The combination of graphene sheets and functional moieties endows GQDs with diverse electrical and electrochemical properties, which will be discussed further in this study.

Beyond composition and morphology, GQDs exhibit high specific surface areas due to their nanoscale properties. In contrast to graphene, which is prone to strong π-π interactions, GQDs, owing to their hydrophilic functional groups, exhibit favorable dispersibility in solution. For instance, Li et al. incorporated N-GQDs into a metal-organic framework (MOF) to fabricate supercapacitors [65]. This integration reduced the composite's contact angle from 125.2° to 81.4° and increased the pore size from 1.7 nm to 4.0 nm. These changes can be attributed to enhanced hydrophilicity and increased specific surface area.

#### 3.1.2. Fluorescence Properties

The fluorescence of GQDs arises from a complex interplay of multiple mechanisms, involving quantum confinement, surface defects, and molecular-state emissions [66−69]. The intrinsic emission originates from band-to-band transitions within the $sp^2$-hybridized carbon core. The size and conjugation degree of the graphene domains determine the optical bandgap through quantum confinement effects [66]. However, the PL behavior of GQDs cannot be fully explained by core-state transitions alone. Surface and edge functionalization introduces localized defect states within the bandgap, resulting in redshifted and excitation-dependent emissions [67]. These defect-related states have been visualized by sub-particle resolution techniques. Recent time-resolved and spectroscopic analyses have demonstrated that surface oxidation and defect reconstruction dynamically alter PL characteristics, reinforcing the dominant role of surface-state engineering [68]. Furthermore, the formation of small organic fluorophores or conjugated fragments during bottom-up synthesis has been identified as an additional 'molecular-state' pathway [69]. This pathway yields excitation-independent, high-efficiency emission, but may obscure the intrinsic properties of GQDs.

Therefore, GQD emissions can be understood as a multichannel process, in which π-domain confinement governs the primary excitation, surface traps and dopants tune emission color, and possible molecular fragments contribute auxiliary luminescence. The broadband and chemically tunable fluorescence properties of GQDs

highlights their potential for diverse optoelectronic applications. Nevertheless, the relative contributions of these pathways remain debated, posing a significant challenge for electroanalytical applications, particularly in ECL and PEC systems, where emission mechanisms directly affect stability, potential-dependent behavior, and sensor sensitivity.

#### 3.1.3. Electrical Properties

The highly π-conjugated system inherited from graphite contributes to the superior electrical conductivity of GQDs. Graphene exhibits remarkable electronic properties in its two-dimensional sheets, owing to the absence of a gap between the valence and conduction bands. When reduced to nanoscale fragments, the number of electrons in the particles decreases from infinite to finite, leading to the splitting of the originally continuous bands. While the emergence of bandgaps may disrupt the ideal graphene structure, they also facilitate more efficient heterogeneous electron transfer at defect sites via tunneling, compared to the perfect basal plane of graphene. Moreover, the band gap and electron density of GQDs can be precisely tuned by introducing heteroatoms, functional groups, or internal defects, making GQDs highly effective as charge transfer accelerators [8,11,70]. For example, Qing et al. demonstrated a simple method to enhance the electrochemical performance of activated carbon (AC) in supercapacitors by incorporating highly crystallized GQDs [70]. GQDs acted as 'electron transfer highways' within the composite, facilitating ion migration and storage in micropores.

#### 3.1.4. Electrochemical Properties

The electrochemical reactivity of GQDs originates from their tunable energy bands and the abundant edge defects, which facilitate heterogeneous electron transfer via a high density of surface states. Additionally, GQD-modified electrodes exhibit increased surface areas and additional binding sites. GQDs also serve as nanocarriers for capturing low-molecular-weight molecules, enabling signal amplification in electrochemical sensors.

The presence of chemical groups and dopants not only creates active sites but also imparts intrinsic electrocatalytic properties. Sun et al. first explored the role of GQD functional groups in the catalytic decomposition of $H_2O_2$ [71]. They found that ketonic carbonyl, carboxyl, and hydroxyl groups function as active sites, substrate-binding sites, and inhibition sites, respectively. GQDs have been employed as electrocatalysts in various reactions, including oxygen reduction, carbon dioxide reduction, and dopamine oxidation [72−74]. Moreover, the nanoscale dimensions of GQDs enable interactions with redox centers of biological enzymes like laccase [75], promoting direct electron transfer. Owing to their chemical inertness, GQDs offer excellent catalytic stability and recyclability [76], making them promising for enhancing catalyst longevity.

The electrochemical properties of GQDs also extend to PEC and ECL processes. Under light excitation, electrons are promoted from the valence band to the conduction band, emitting photoluminescence (PL) upon relaxation. GQDs typically exhibit a broad absorption spectrum in the ultraviolet range, sometimes extending into the visible spectrum. In PEC processes (Figure 3A) [77], light energy is converted into photoelectrons, and variations in the chemical environment of the surrounding solution can modulate the photocurrent, enabling sensitive detection [20,21]. In ECL processes (Figure 3B), high-energy electrons, rather than light sources, induce luminescence. The first co-reaction ECL system using GQDs as emitters was reported in 2012 [78]. Due to the quantum size effect, the energy gap of the surface state (for ECL emissions) is narrower than that of the core (for PL emissions), leading to slight shifts in the emission wavelengths between ECL and PL.

### *3.2. Property Regulations*

Most regulation strategies focus on modifying the band gap or electron density of GQDs, typically through size adjustment, doping with heteroatoms, and the introduction of functional groups. Notably, functional groups are often introduced alongside doping, which can also affect GQD size. Although these modifications are frequently considered separately, their effects are inherently interconnected. In addition to compositional modifications, the arrangement of GQDs, whether self-assembled or combined with other nanomaterials, can also impact their electrochemical properties. The following section discusses regulatory strategies for tuning the electrochemical properties of GQDs, including size control, functionalization, doping, and assembly approaches.

#### 3.2.1. Size

The energy gap and electronic properties of GQDs are strongly dependent on their size due to the quantum size effect. As shown in Figure 4A [79], the energy band broadens as the size decreases, a phenomenon reflected in the PL blue shift of GQDs. The size of GQDs can be adjusted by altering synthesis conditions such as

temperature [80], applied potential [81], reactant concentrations [82], and reaction time [83], or through post-synthesis treatments like membrane filtration [84]. Li et al. successfully synthesized three N-GQD samples of different sizes but with similar functional groups using an organic chemistry approach, demonstrating their potential for catalyzing the ORR [27]. Larger N-GQDs exhibited enhanced catalytic activity, as indicated by an increase in cathodic current density. It is worth noting that face-to-face interactions become more pronounced with increasing GQD size, reducing solubility, and limiting the range of stable GQD sizes [33].

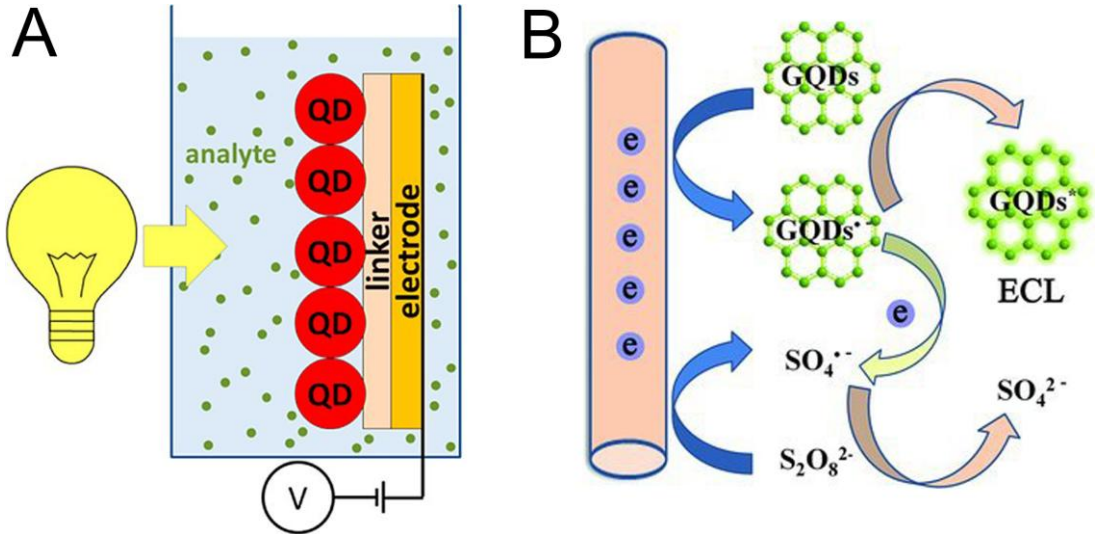


**Figure 3.** Operational mechanisms of GQD-based PEC and ECL sensors. (**A**) Operational principle of a quantum dot-based PEC sensor. Reproduced with permission [77]. Copyright 2013, American Chemical Society. (**B**) Proposed ECL mechanism of GQDs with K2S2O8 serving as a co-reactant. Reproduced with permission [78]. Copyright 2012, WILEY-VCH.

### 3.2.2. Functionalization

The presence of functional groups with electron-donating or electron-withdrawing properties has a significant impact on the band gap, redox state, and electron redistribution within GQDs. A variety of functional groups have been utilized to modify GQDs, with the objective of enhancing their electrochemical activity, including histidine, dimercaprol, hydroxyl, carboxyl, sulfhydryl, and hydrazine [12,13,62,63,71,85]. The functionalization of GQDs can be achieved via two main strategies: covalent coupling with residues or non-covalent interactions. As shown in Figure 4B, electron-donating groups facilitate charge transfer from the functional groups to the core of GQDs, resulting in an electron-dense structure and a reduction in the band gap, while electron-withdrawing groups produce the opposite effect [86]. Functionalization is a prevalent method for regulating emissions, though its effects may differ between PL and electrochemical systems. For instance, Li et al. synthesized two GQDs with similar sizes but different oxidizing group contents [78]. The GQDs with higher oxidizing group content exhibited decreased PL but enhanced ECL. This phenomenon is attributed to the functional groups, which narrow the bandgap and promote non-radiative recombination in PL. In ECL systems, these groups are converted to active free radicals, facilitating efficient co-reactant generation and enhancing ECL emission.

In addition to modulating band gaps, functional groups alter the dipole moment of GQDs, enhancing the reactivity of delocalized electrons and increasing their propensity for electrostatic interactions and chemical bonding. The extent of dipole moment variation depends on the type and number of functional groups. This modification can also be used to improve the affinity of GQDs for solvent molecules and other reactants [87]. Esmaeili et al. demonstrated the sensitive detection of trace mercury ions using dimercaprol-functionalized GQDs on modified GCEs. The pre-concentration of mercury ions is driven by the affinity between the dimercaprol groups and $Hg^{2+}$ ions [13].

Moreover, targeted functional group modification has been shown to impart designated catalytic activity and selective recognition capabilities to GQDs. Sun et al. reported the roles of carbonyl, hydroxyl, and carboxyl groups in the catalytic degradation of $H_2O_2$, highlighting the potential for constructing artificial nano-enzymes [71]. Another study showed that histidine- and DNA-functionalized GQDs can be used for the electrochemical detection of chlorpyrifos based on specific hybridization [88].

### 3.2.3. Doping

The doping of heteroatoms can be achieved via two main approaches: top-down cutting and bottom-up synthesis from precursors containing the desired dopants. Post-synthesis methods have also been explored, although they generally exhibit lower efficiency [89]. As shown in Figure 4C, heteroatoms such as N, S, B, P, F, and Se [27,61,90−94] have been employed to modulate the properties of GQDs. Among these, nitrogen is the most common dopant due to its atomic size similarity to carbon and its five valence electrons suitable for bonding. Dopants with different electronegativities alter the electron density distribution within the π-conjugated system, thereby enhancing GQD reactivity [95]. For instance, Chowdhury et al. prepared N,S-GQDs via a hydrothermal method for virus detection based on impedance analysis [61], where nitrogen improved electrochemical activity by modulating electronic distribution, and sulfur increased the number of anchoring sites for adsorption onto noble metal nanoparticles. Lima synthesized a self-organized 2D network of B-functionalized N-GQDs (B,N-GQDs) for dopamine detection [96]. The B,N-GQDs lowered the oxidation and reduction potentials of dopamine and enhanced sensor sensitivity through favorable interactions between boric acid and diols.

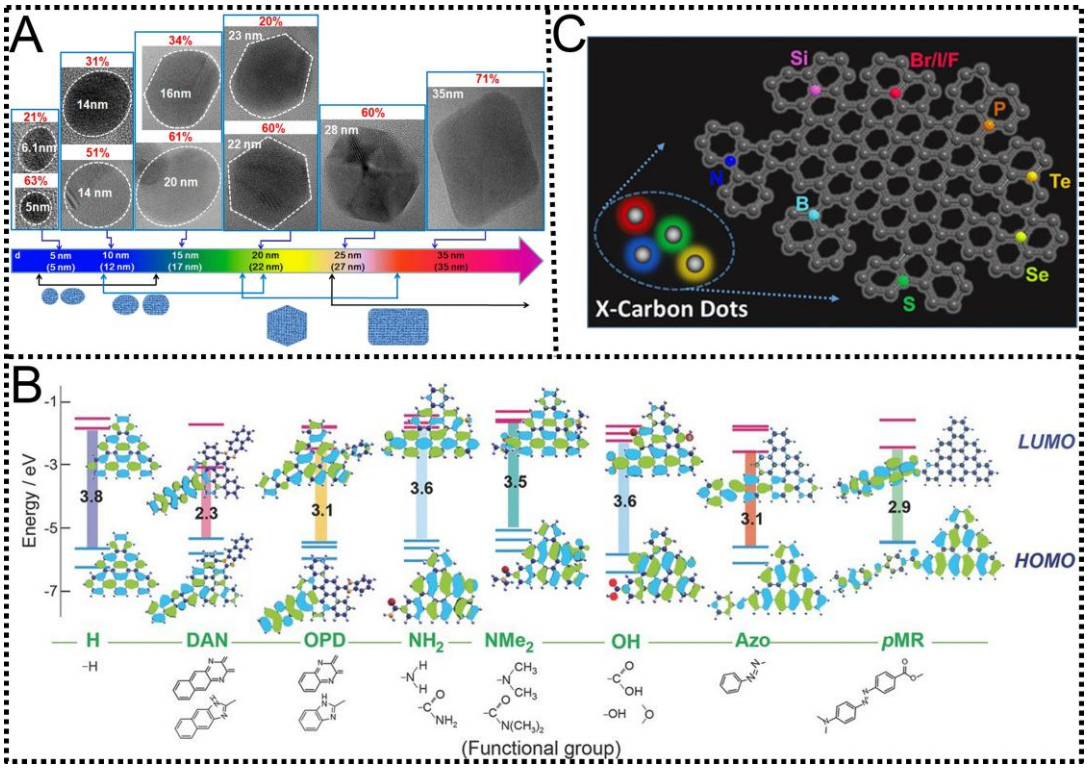


**Figure 4.** Strategies for tailoring the properties of GQDs through size control, functionalization, and heteroatom doping. (**A**) HRTEM images of GQDs showing size- and shape-dependent populations. Reproduced with permission [79]. Copyright 2012, American Chemical Society. (**B**) Predicted energy level diagrams of graphene functionalized with electron-donating and electron-withdrawing groups. Reproduced with permission [86]. Copyright 2016, WILEY-VCH. (**C**) Illustrative examples of heteroatom-doped GQDs for property modulation. Reproduced with permission [90]. Copyright 2019, WILEY-VCH.

### 3.2.4. Assembly and Composites

The arrangement of GQDs and their interactions with other materials are critical factors for property modulation. For example, Vázquez-Nakagawa et al. demonstrated the assembly of chiral fluorescent GQDs via amide hydrogen bonding and π-π stacking interactions [28]. The resulting fibrous structure enhanced electronic coupling between individual GQDs. Cheng et al. constructed GQD-based nanotubes as a Raman platform for detecting 2,4-dinitrotoluene [97]. The nanotube stacking facilitated efficient electron transport, while the ordered micropores and hollow structure increased reactant accessibility. Xu et al. fabricated a nanoenzyme via electrodeposition in ionic liquid electrolytes, densely assembling GQDs onto flexible carbon fibers for electrochemical $H_2O_2$ detection [11].

Integration into composites has been shown to overcome the intrinsic limitations of GQDs while providing multiple advantages. The high solubility of GQDs presents challenges for their immobilization on electrode surfaces, which can be effectively addressed by combining GQDs with metal nanomaterials [98,99]. Additionally,

Du et al. prepared a composite film of poly(3,4-ethylene-dioxythiophene):polystyrenesulfonate (PEDOT:PSS) and GQDs via electrostatic and π-π interactions, resulting in significantly improved conductivity and thermoelectric properties of PEDOT:PSS. Jiang et al. developed a PEC sensor for *E. coli* using a heterojunction of $WO_3 \cdot H_2O$ and N-GQDs [100]. The localized plasmon resonance of $WO_3 \cdot H_2O$ expanded light absorption from visible to near-infrared wavelengths, substantially enhancing the photocurrent through efficient charge transfer within the heterojunction.

## 4. Applications of GQDs in Electroanalysis

The advantages of simple instrumentation, rapid response, and high sensitivity have driven extensive research in electroanalysis. GQDs, owing to their unique properties and precise modifications, play multiple roles across electrochemical, ECL, and PEC sensing platforms. A critical consideration in designing GQD-based sensors is that the chosen sensing technique dictates which GQD properties are most effectively leveraged. In electrochemical sensors, the high conductivity and large specific surface area of GQDs are crucial for signal amplification. In ECL sensors, tunable energy bands and surface states are essential for efficient luminescence generation or quenching. For PEC sensors, broadband light absorption and efficient charge separation are key assets. Nonetheless, challenges remain: the inherent solubility of GQDs complicates stable electrode immobilization, often necessitating composite structures, and the lack of standardized GQD materials hampers direct performance comparisons across studies. The following sections will examine the applications of GQDs in electroanalysis, highlighting their multifaceted roles as carriers, signal amplifiers, electrocatalysts, emitters, co-reactants, and photosensitizers. These roles enable the sensitive detection of ions (e.g., $Cd^{2+}$, $Hg^{2+}$, $Pb^{2+}$, $Zn^{2+}$, $Cr^{6+}$, $Cu^{2+}$, $S_2O_8^{2-}$) [9,13,101−103], molecules (e.g., dopamine, $H_2O_2$, purine bases, amino acids, flutamide, caffeic acid, acetamiprid) [8,11,12,19,104,105], biological macromolecules (e.g., proteins, antigens, lysozyme, DNA, miRNA) [10,14,17,18,21], cells [15,100], and viruses [16,20]. GQD-based electroanalysis has found widespread applications in environmental monitoring, food safety, clinical diagnosis, and biosensing.

### *4.1. Electrochemical Sensors*

The application of GQDs in electrochemical sensors has attracted considerable attention due to their abundant conjugated electrons, high surface area, and multiple accessible active sites. Despite numerous reports, the roles of GQDs in electrochemical sensors can be broadly classified as: (i) facilitating material integration, (ii) promoting interfacial charge transfer, and (iii) acting as nanocatalysts.

As illustrated in Figure 5A, Bhatnagar et al. developed an electrochemical sensor for differential pulse voltammetry (DPV) detection of cardiac troponin I (cTnI) [14], where GQDs served as both connectors and signal amplifiers. GQDs were coupled with a gold electrode and dendritic PAMAM via EDC-NHS and carbodiimide coupling, respectively. This nanocomposite provided abundant binding sites for anti-cTnI and cTnI, efficiently enhancing signal intensity and sensitivity. Similarly, Arumugasamy et al. employed GQDs conjugated with cTnI as a receptor for immunosensing, achieving a detection limit of 29 pM [106]. Ganganboina et al. reported impedimetric detection of glioma cells using S-doped GQDs@gold-carbon nanospheres, where GQDs were linked with antibodies and gold-carbon nanospheres to enhance probe activity (Figure 5B) [15]. Li et al. fabricated a self-powered sensing platform for monitoring uric acid in sweat using a cobalt nanocrystal-GQDs-$Ti_3C_2T_X$ monolithic film [107], in which GQDs acted as a crosslinking agent. The small size, multiple functional groups, and strong positive charge of GQDs influenced the viscosity of the $Ti_3C_2T_X$ hydrogel and promoted uniform dispersion of cobalt nanocrystals through coordination.

GQDs further enhance interfacial charge transfer owing to their unique electrical properties and abundant defects. For example, Cotchim et al. developed an activated carbon-based, unlabeled electrochemical immunosensor for quantifying prostate-specific antigen (PSA) [108]. The activated carbon modified with GQDs exhibited optimal electron transfer characteristics. Zahed et al. designed an electrochemical sensor for the sensitive detection of the cytostatic drug flutamide, in which a GCE was modified with GQDs and hierarchical flower-like gold nanostructures (HFGNs) to increase surface area and electron transfer rate [109]. Yang et al. reported a sandwich-type electrochemical immunosensor for PSA detection [110], employing N-GQDs functionalized with gold nanoparticles via a hydrothermal process to accelerate electron transfer and enhance antibody immobilization, as illustrated in Figure 5C.

GQDs also exhibit specific catalytic capabilities in certain applications. For instance, Prasad et al. utilized N-acryloyl-4-aminobenzamide-functionalized GQDs to construct an electrochemical sensor for detecting the anticancer drug ifosfamide (IFO), as shown in Figure 5D [111]. GQDs were found to lower the oxidation overpotential of the analyte, thereby enhancing electrode kinetics and electrocatalytic activity. Similarly, Gu et al.

synthesized highly amidized GQDs as metal-free catalysts for electrochemical $H_2O_2$ detection. The GQD-modified electrode facilitated $H_2O_2$ adsorption and reduction, achieving a high selectivity of 1.83 $\mu A \cdot mM^{-1} \cdot cm^{-2}$ over a concentration range of 0.5–40 mM [112].

Finally, the multifaceted role of GQDs in enhancing electrochemical sensor performance should be emphasized. For example, Xu et al. developed a double-nanometer enzyme electrochemical sensor for the sensitive detection of $H_2O_2$ [11]. GQDs promoted the growth of Au-Pd nanoparticles (AuPd-ANPs) while simultaneously restricting the formation of high-density, ultra-fine Au-Pd NPs through quantum confinement and edge effects. Additionally, GQDs acted as nano-enzymes, exhibiting synergistic electrocatalytic activity toward $H_2O_2$ in combination with Au-Pd NPs. The corresponding schematic and TEM image of AuPd-ANPs/GQDs are shown in Figure 5E.

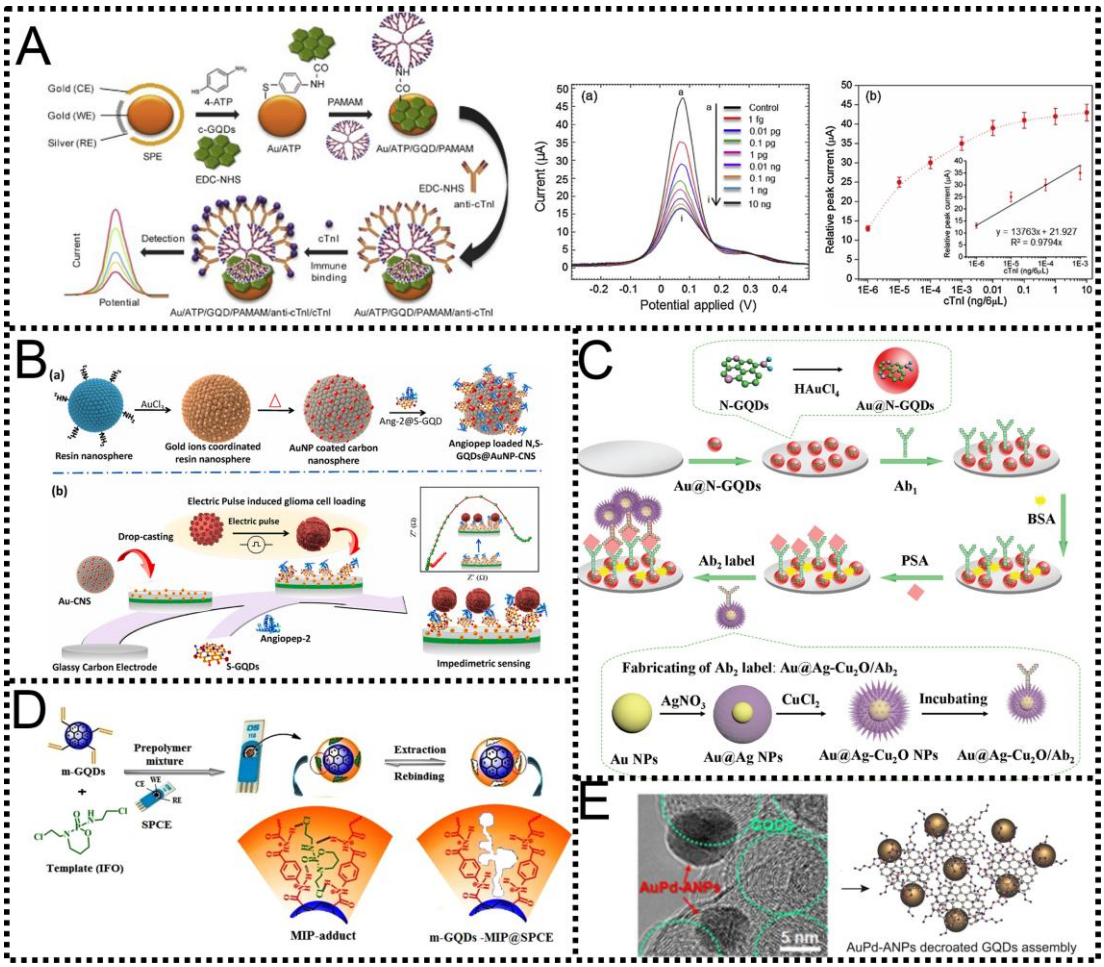


**Figure 5.** Multifunctional roles of GQDs in electrochemical sensors for detecting biomarkers and small molecules. (**A**) Schematic illustration and DPV responses of an electrochemical sensor based on GQDs-PAMAM nanohybrid modified gold electrode for the detection of cTnI. Reproduced with permission [14]. Copyright 2016, Elsevier B.V. (**B**) Fabrication process and pulse-induced impedimetric detection of glioma cells using S-doped GQDs@gold-carbon nanospheres. Reproduced with permission [15]. Copyright 2021, Elsevier B.V. (**C**) Construction and detection process of a sandwich-type electrochemical immunosensor for PSA. Reproduced with permission [110]. Copyright 2017, Elsevier B.V. (**D**) The illustration for the fabrication of the electrochemical sensor for IFO detection. Reproduced with permission [111]. Copyright 2017, Elsevier B.V. (**E**) TEM image and illustration of the AuPd-ANPs/GQDs in the double nano-enzyme sensor for the sensitive detection of $H_2O_2$. Reproduced with permission [11]. Copyright 2018, Elsevier B.V.

### *4.2. ECL Sensors*

ECL has gained widespread attention over recent decades owing to its high sensitivity, broad dynamic range, and facile modulation. GQDs have been shown to enhance ECL performance by providing reaction sites and facilitating charge transfer, similar to their role in electrochemical sensors. In addition, their excellent electronic properties, tunable energy bands, and high quantum efficiency make them promising ECL emitters. The first co-

reactant ECL system employing GQDs as the cathodic emitter was reported in 2012 [78]. Compared with CQDs, GQDs, particularly single-layer variants, possess higher specific surface areas, suggesting greater potential as ECL sensitizers [102]. For example, Dong et al. demonstrated a co-reactant ECL system in which GQDs functioned as the emitter for lead ion detection, as illustrated in Figure 6A. The cathodic ECL signal depends on cysteine oxidation, dissolved oxygen, and GQD reduction [102]. Nie et al. developed an immunoassay ECL sensor using GQDs@AuNPs for carcinoembryonic antigen (CEA) detection. As shown in Figure 6B, the amount of GQDs@AuNPs bound to the electrode via antigen-antibody interactions correlates with the CEA concentration [18].

GQDs can also act as co-reactants, exhibiting an enhancement mechanism similar to that of small molecules [113]. Long et al. reported the first use of GQDs as co-reactants in the anodic ECL of $Ru(bpy)_3^{2+}$ [19], as shown in Figure 6C. The benzylic alcohol units on GQDs were oxidized to reductive radical intermediates, which facilitate the reduction of electrogenerated $Ru(bpy)_3^{3+}$ to $Ru(bpy)_3^{2+*}$, producing strong ECL emission. This emission was quenched by dopamine oxidation products, indicating potential for bioanalytical applications. Fan et al. incorporated N-GQDs and $Ru(bpy)_3^{2+}$ into $SiO_2$ to fabricate a nanocomposite with self-enhanced ECL, as depicted in Figure 6D. In this system, N-GQDs served as co-reactants, enabling sensitive detection of matrix metalloproteinases [114].

GQDs have been shown to be cost-effective, highly soluble, and readily functionalized. These attributes suggest their potential as alternatives to conventional ECL materials, addressing concerns over the toxicity and biocompatibility of organic fluorophores and semiconductor quantum dots [115]. A summary of reports on GQD-based ECL sensors from the past five years is provided in Table 1.

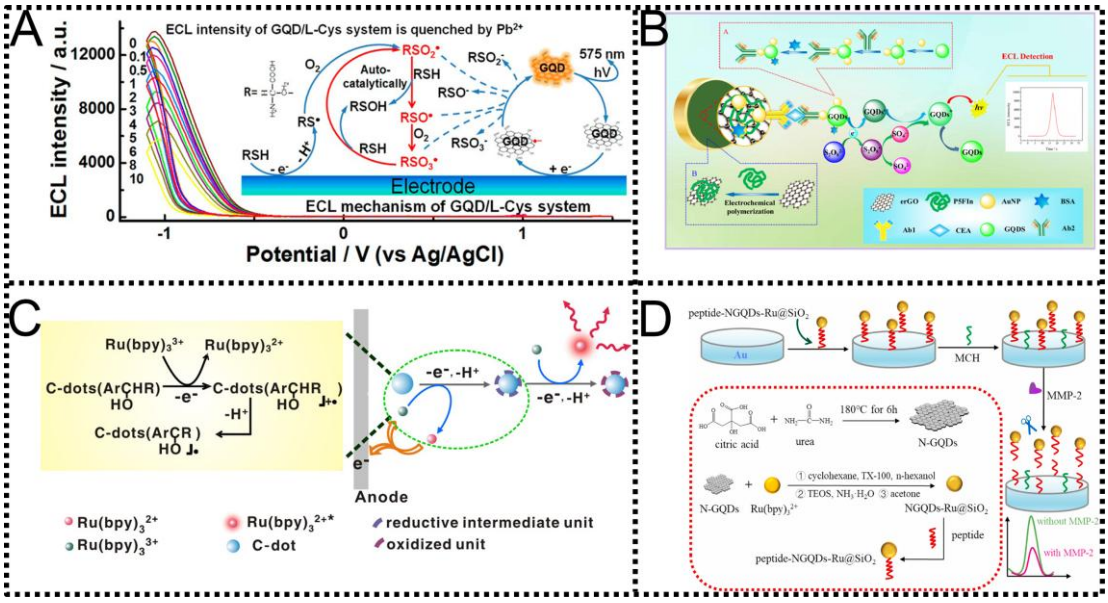


**Figure 6.** GQDs as emitters and co-reactants in ECL sensing platforms. (**A**) The illustration for the reaction mechanism of the GQDs-cysteine ECL system and the response signals in the detection of lead ions. Reproduced with permission [102]. Copyright 2014, American Chemical Society. (**B**) The illustration for the ECL sensor based on GQDs@AuNPs for the sensitive detection of CEA. Reproduced with permission [18]. Copyright 2017, Elsevier B.V. (**C**) The reaction mechanism of anodic ECL of $Ru(bpy)_3^{2+}$ with GQDs as the co-reactant. Reproduced with permission [19]. Copyright 2014, American Chemical Society. (**D**) The illustration of the synthesis of a nanocomposite and the fabrication of the self-enhanced ECL biosensor. Reproduced with permission [114]. Copyright 2021, Elsevier B.V.

**Table 1.** Recently reported GQD-based ECL sensors.

| GQDs Type | Synthesis Method | Analyte | Detection Range | LOD | Role of GQDs | Reference |
|---|---|---|---|---|---|---|
| GQDs | $HNO_3$-treatment of single-walled carbon nanotubes | human chorionic gonadotropin | 2–100 μg/L | 0.21 μg/L | ECL emitter | [116] |
| N, S-GQDs | Pyrolysis using citric acid and cysteine | catechol | 0.01–1000 μM | 0.0082 μM | ECL emitter | [117] |
| N, S-GQDs | Pyrolysis using citric acid and cysteine | tryptophan | 0.01–1000 μM | 0.0066 μM | ECL emitter | [117] |
| N-GQDs | Pyrolysis using citric acid and urea | DNA | 10 fM–10 nM | 8 fM | ECL emitter | [118] |
| N-GQDs | Pyrolysis using citric acid and urea | $Cu^{2+}$ | 0.01–1000 μM | 0.18 μM | ECL emitter | [119] |
| N, Zn-GQDs | Hydrothermal decomposition of GO | cTnI | 0.01–1000 μg/L | 4.59 pg/L | ECL emitter | [120] |
| N-GQDs | Hydrothermal method | cTnI | 0.01–100 μg/L | 2.90 pg/L | ECL emitter, a connector for an antibody | [121] |
| N-GQDs | Hydrothermal method | catechol | 100 nM–10 μM; 10 μM–60 μM | 42 nM | ECL emitter | [122] |
| ZnNCs-N-GQDs | Hydrothermal synthesis with ZnNCs doping | $Hg^{2+}$ | 1 mM–10 pM | 3 pM | ECL emitter | [123] |
| B, N-GQDs | Boric acid and ammonia treatment of GO | microcystin-LR | 0.01–5000 pM | 0.003 pM | ECL emitter | [124] |
| $MoS_2$-GQDs | MoS-GQDs with carboxyl as active sites | DNA | 100 aM–1 nM | 25.1 aM | ECL emitter | [125] |
| N-GQDs | Hydrothermal method under alkaline conditions | $H_2O_2$ | 0.3–100 μM | 63 nM | ECL emitter | [126] |
| N-GQDs | Hydrothermal method under alkaline conditions | glucose | 0.7–90 μM | 96 nM | ECL emitter | [126] |
| N, S-GQDs | Pyrolysis of cysteine and citric acid | ascorbic acid | 10–360 nM | 3.3 nM | ECL emitter in a dual luminescent system | [127] |
| N-GQDs | Hydrothermal method | $Hg^{2+}$ | $5.0 \times 10^{-11}$ M–$1.0 \times 10^{-6}$ M | $3.0 \times 10^{-11}$ M | ECL emitter | [128] |
| GQDs | Acid etching of carbon fiber | miRNA | 100 aM–1 nM | 96 aM | Synergistical ECL emission | [129] |
| Immobilized GQDs | $HNO_3$-treatment of multi-walled carbon nanotubes | 5-Fluorouracil | 0.0005–500 μg/L | 0.17 ng/mL | ECL donor | [130] |
| N-GQDs | Hydrothermal method | procalcitonin | 0.0001–100 μg/L | 12.58 pg/L | ECL donor | [131] |
| GQDs | Hydrothermal decomposition of GO | cTnI | 500 pg/L–20 μg/L | 354.2 pg/L | ECL donor | [132] |
| GQDs | Hydrothermal method | $Cu^{2+}$ | 0.5–1000 nM | 0.37 nM | Anode ECL referenc | [133] |
| N-GQDs | Hydrothermal method | acetamiprid | 1 pM–10 nM | 0.056 pM | Co-reactant | [134] |
| N, S-GQDs | Electrolysis of graphene | okadaic acid (OA) | 0.003–40 μg/L | 0.001 μg/L | Co-reactant | [135] |
| GQDs | Oxidation of graphene sheets in piranha solution | lysozyme | 10 fM–10 nM | 0.8 fM | Co-reactant | [136] |
| N-GQDs | Hydrothermal method | deoxynivalenol (DON) | $1.0 \times 10^{-15}$–$5.0 \times 10^{-8}$ g/mL | $8.5 \times 10^{-16}$ g/mL | Co-reactant | [137] |
| N-GQDs | Acid treatment of N-graphene aerogel | ochratoxin A (OTA) | $10^{-5}$–1 μg/L | 0.2 ng/L | Co-reactant | [138] |
| N-GQDs | Hydrothermal method | $Hg^{2+}$ | $10^{-14}$–$10^{-6}$ M | 3 fM | Co-reactant | [139] |
| N-GQDs | Hydrothermal method | aflatoxin B1 | $3 \times 10^{-5}$–$1 \times 10^{2}$ μg/L | $3 \times 10^{3}$ μg/L | Co-reactant | [140] |
| N-GQDs | Hydrothermal method | matrix metalloproteinases-2 | 0.01–185 μg/L | 6.5 ng/L | Co-reactant | [114] |
| N-GQDs | Hydrothermal method | carbohydrate antigen (CA) 199 | 0.5 mU/mL–50 U/mL | 0.03 mU/mL | Co-reaction accelerator | [141] |
| N-GQDs | Hydrothermal method | CA 125 | 0.5 mU/mL–500 U/mL | 0.005 mU/mL | Co-reaction accelerator | [141] |
| N-GQDs | Hydrothermal method | CEA | 0.00001–40 μg/L | 0.269 pg/L | Quenching luminol, binding with $Cu_2S$ | [142] |

### *4.3. PEC Sensors*

GQDs, owing to their unique optical and electrochemical properties, can also serve as photosensitive materials in PEC sensors. Target analytes can influence PEC signals in two ways: by participating in the photoelectric conversion process and by consuming the generated charge carriers. For example, Pang et al. developed a heterojunction-sensitized PEC sensor for hepatitis B virus (HBV) DNA [21]. N-GQDs/g-$C_3N_4$ heterojunctions acted as sensitizers, compensating for the narrow band gap of $TiO_2$, suppressing photocarrier recombination, and enhancing photocurrent conversion efficiency. Zheng et al. synthesized boron- and GQD-codoped g-$C_3N_4$ for selective dopamine detection, as illustrated in Figure 7 [143]. The doping facilitates photogenerated electron transfer from the conduction band of g-$C_3N_4$ to GQDs, improving charge separation and broadening light absorption. Additionally, GQDs can function as signal quenchers in PEC sensors. Meng et al. reported a signal-off PEC sensor for detecting M.SssI MTase enzyme activity [144]. GQDs embedded in ZIF-8 on the electrode impeded the photocurrent signal due to steric hindrance. Moreover, GQDs acted as peroxidase mimetics, catalyzing the precipitation of 4-chloro-1-naphthol, which substantially decreased the photocurrent. A summary of reports on GQD-based PEC sensors over the past five years is provided in Table 2.

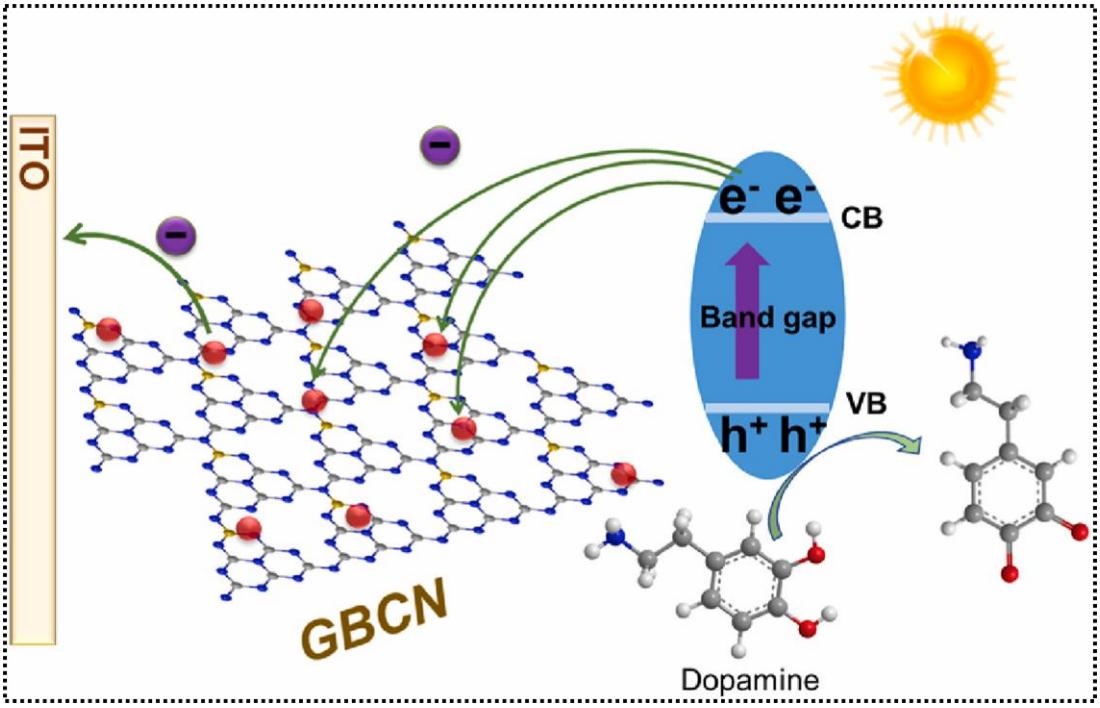


**Figure 7.** Schematic illustration of a PEC aptasensor for dopamine detection based on a boron-GQD-g-$C_3N_4$ composite. Reproduced with permission [143]. Copyright 2023, Elsevier B.V.

**Table 2.** Recently reported GQD-based PEC sensors.

| GQDs Type | Synthesis Method | Analyte | Detection Range | LOD | Role of GQDs | Reference |
|---|---|---|---|---|---|---|
| GQDs | Hydrothermal method | di-2-ethylhexyl phthalate | 0.3–100 ng/L | 0.1 ng/L | Photosensitizer | [145] |
| GQDs | Commercial suspension | $Cr^{6+}$ | 0.08–100 μM | 0.04 μM | Photosensitizer | [146] |
| N, S-GQDs | Hydrothermal method | di-2-ethylhexyl phthalate | 0.1–5 μM; 5–1380 μM | 36 nM | Photosensitizer, anchoring aptamer | [147] |
| S, N-GQDs | Hydrothermal method | bisphenol A | 0.12–5 μM; 5–40 μM | 0.04 μM | Enhancing charge transfer | [148] |
| N-GQDs | Pyrolysis | ascorbic acid | 0.1–$10^4$ CFU/mL | 0.05 CFU/mL | Enhancing charge transfer | [149] |
| GQDs | Hydrothermal method | dopamine | 0.001–800 μM | 0.96 nM | Enhancing charge transfer, extending absorption, and providing adsorption sites for dopamine | [143] |
| N-GQDs | Hydrothermal method | *E. coli* | 1 nM–800 μM | 0.96 nM | Enhancing charge transfer, extending absorption | [100] |

### *4.4. Integrated Assessment*

Although the diversity of analytes limits direct comparison of absolute performance metrics, the collective evidence clearly establishes GQDs as a versatile, high-performance platform for electrochemical analysis. As summarized in Tables 1 and 2, GQD-based sensors typically achieve detection limits ranging from the nanomolar to sub-nanomolar level, with linear dynamic ranges spanning two to five orders of magnitude. These performances are comparable to or surpass those of conventional carbon nanomaterials, such as graphene oxide and carbon nanotubes. Representative examples include attomolar ($10^{-18}$ M) detection of nucleic acids [125,129], picomolar-level detection of biomarkers such as cTnI (29 pM, [106]), and broad micromolar-to-millimolar ranges for small-molecule analytes such as $H_2O_2$ (0.5–40 mM, [112]). As shown in Table 3, a comparative evaluation using $H_2O_2$ as a model analyte further demonstrates how electronic-structure tuning, surface functionalization, and interfacial engineering collectively dictate the electrochemical behavior of GQDs.

**Table 3.** GQD-based electroanalysis for $H_2O_2$ detection.

| GQDs Type | Sensing Method | Detection Range | LOD | Response Time | Reference |
|---|---|---|---|---|---|
| N,S-GQD/Graphene | Electrocatalytic reduction | 0.4 μM–33 mM | 26 nM | ~3 s | [150] |
| N-GQD@N-doped carbon hollow nanosphere | Electrocatalytic reduction | up to 1.4 mM | 20 nM | <2 s | [151] |
| Au NPs-N-GQDs | Electrocatalytic reduction | 0.25 μM–13.3 mM | 0.12 μM | ~5 s | [152] |
| N-GQDs@$SnS_2$ nanocomposite | Electrocatalytic reduction | 0.0125–1128 μM | 9 nM | ~3 s | [153] |
| Highly amidised N-GQDs | Electrocatalytic reduction | 0.5–40 mM | – | – | [112] |
| AuPd NPs/GQDs | Electrocatalytic reduction | 1.0 μM–18.44 mM | 500 nM | – | [11] |
| GQDs | ECL quenching | 10–100 μM | 3.0 μM | 30 min | [154] |
| N-GQDs | ECL enhancement | 0.3–100.0 μM | 63 nM | – | [126] |
| Luminol-N-GQDs | ECL resonance energy-transfer (RET) | 0.033–74 μM | 10 nM | – | [155] |

Atomic-level doping underpins the intrinsic catalytic activity of GQDs. Nitrogen incorporation generates pyridinic and graphitic N sites, disrupts lattice neutrality, and creates highly active centers. Highly amidized N-GQDs [112], for example, achieve metal-free catalysis toward $H_2O_2$ with a sensitivity of 1.83 $\mu A \cdot mM^{-1} \cdot cm^{-2}$. Co-doping with sulfur further delocalizes π-electrons, lowering the detection limit to 26 nM and extending the linear range across five orders of magnitude [150]. Molecular functionalization can additionally redefine sensing mechanisms. In ECL systems, a cathodic GQD/$SO_3^{2-}$ sensor (LOD = 3.0 μM, [154]) relies on an external co-reactant, whereas an anodic N-GQD-luminol hybrid (LOD = 63 nM, [126]) exhibits intrinsic co-reactivity and markedly enhanced emission. The incorporation of hydrazide or amide groups into the GQD framework thus modifies radiative pathways and substantially enhances performance.

Hybridization with complementary nanomaterials induces synergistic improvements in conductivity, catalysis, and energy transfer. For instance, N,S-GQD/graphene composites establish efficient electron-transfer networks, enabling rapid responses of approximately 3 s [150]. The inclusion of noble metal components further introduces highly active catalytic centers, as demonstrated by N-GQD@N-doped carbon hollow nanospheres [151] and AuPd-NP/GQD hybrids [11], which achieve detection limits of 20 nM and sensitivities up to 371 $\mu A \cdot mM^{-1}$ $cm^{-2}$, respectively. Moreover, luminol-N-GQD composites [155] combine covalent functionalization with a RET process, producing red-shifted and significantly intensified ECL emission with an ultralow detection limit of 10 nM. Collectively, these findings illustrate how interfacial engineering enables multi-level cooperation, enhancing charge transport, catalytic activity, and optical response to maximize analytical performance.

Overall, the development of GQD-based electroanalytical systems demonstrates a clear progression: from single-parameter optimization to synergistic multi-factor design, from empirical modifications to rational molecular engineering, and from broad applicability to mechanism-driven precision tuning. Elucidating these structure-property-function relationships provides a robust framework for the design of next-generation electroanalytical sensors.

In parallel with these scientific advancements, evaluating the commercial potential of GQD technologies is crucial. Their outstanding analytical performance positions them as compelling alternatives to conventional carbon nanomaterials. The commercial appeal of GQDs arises from three key advantages: (i) low-cost synthesis from abundant carbon precursors, providing an economic advantage over noble-metal- or rare-earth-based materials; (ii) inherent biocompatibility and low toxicity, allowing safe use in real-time and in vivo biosensing applications; and (iii) multifunctionality, as individual GQDs can simultaneously facilitate signal transduction, molecular recognition, and catalysis, thereby streamlining device design and fabrication. Despite these advantages, the commercial translation of GQDs remains limited by challenges related to long-term stability and reproducibility.

Notably, progress has been made in addressing these issues. For example, a N-GQD/NiCo-layered double hydroxide hybrid electrode retained approximately 81.7% of its initial sensitivity after 30 days of storage at room temperature, indicating promising durability for practical applications [156]. Likewise, a GQD-AuNP composite immunosensor achieved recovery rates of 97–105% in human serum samples for S-100B detection, demonstrating excellent anti-interference performance and reliability in complex biological matrices [157]. Although preliminary, these findings provide compelling evidence that GQD-based devices can achieve the stability and reliability required for practical deployment.

A clear understanding of the performance trade-offs among different sensing modes is essential for guiding future commercialization. Electrochemical sensors, noted for their simplicity and cost-effectiveness, are well-suited for portable or disposable point-of-care devices. ECL sensors, offering ultrahigh sensitivity and precision, are ideal for advanced diagnostics but necessitate complex optical setups. PEC sensors, which leverage dual photoelectric control and exhibit low background noise, show promise for miniaturized analytical systems, though careful management of ambient light sensitivity is required.

Looking ahead, combining machine-learning-assisted material design with high-throughput experimentation will expedite the identification of optimal GQD structures for specific applications. Concurrently, the development of green, continuous-flow synthesis methods will be crucial for scalable, reproducible, and cost-effective production. Once challenges in stability and consistency are addressed, GQD-based electroanalytical technologies are poised to transition from proof-of-concept demonstrations to commercially competitive platforms for point-of-care diagnostics, environmental monitoring, and other emerging applications.

## 5. Summary and Prospect

Various synthetic and regulatory methods endowed GQDs with distinct optical, electrical, and electrochemical properties that enable their multifunctional roles in electroanalysis. This paper systematically reviews these multifunctional roles, establishing a function-oriented framework. Despite the significant progress, the field of GQD-based electroanalysis faces several critical challenges that must be addressed to transition from laboratory demonstrations to practical applications.

(a) Synthesis and Purification: The predominant reliance on severe reagents or energy-consuming processes stands in opposition to the fundamental tenets of green chemistry and gives rise to concerns regarding scalability. A more pressing issue lies in the frequent presence of by-products and the absence of standardized purification protocols, which compromise the reliability of reported electrochemical properties, as signals may originate from molecular impurities rather than the GQDs themselves.

(b) Structure-Property Relationship: While the optical properties of GQDs have been extensively mapped, a quantitative understanding of how specific structural features (e.g., degree of crystallinity, spatial distribution of dopants) govern electrochemical properties (e.g., charge transfer resistance, electrocatalytic overpotential) remains deficiently explored. The employment of advanced in situ/operando characterization techniques has the potential to address this knowledge gap.

(c) Performance Optimization: The expansion of the PL range and the enhancement of quantum yield are frequently pursued objectives. In electroanalysis, however, a more targeted objective is the rational design of GQDs with tailored band gaps and surface states to maximize the efficiency of specific electrochemical processes, such as co-reactant pathways in ECL or hole-electron separation in PEC.

(d) Multifunctionality: Beyond the exploration of optical and electrical properties, the exploration of other characteristics, such as the magnetic properties of metal-doped GQDs, remains underexplored. The integration of multiple functionalities into a single GQD-based platform may unlock novel sensing modalities, thereby pushing the boundaries of current detection strategies.

(e) Safety: Despite being frequently promoted as nontoxic, there is some evidence indicating size-dependent toxicity [158]. Systematic studies on biodistribution, degradation, and long-term effects are necessary for the utilization of GQDs in vivo or for their release into the environment.

## Funding

We thank the support of the National Natural Science Foundation of China (22174061). This work was also supported by the National Natural Science Foundation of China (22304086), and the Start-Up Fund from NJUPT (NY223051), the Natural Science Foundation of the Jiangsu Higher Education Institutions of China (23KJB150025), the Research Fund from the Key Laboratory for Organic Electronics & Information Displays (GZR2023010045), and the Foundation of State Key Laboratory of Analytical Chemistry for Life Science (SKLACLS2311).

## Conflicts of Interest

The authors declare no conflict of interest.

## Use of AI and AI-assisted Technologies

No AI tools were utilized for this paper.

## References


1. Ponomarenko, L.A.; Schedin, F.; Katsnelson, M.I.; et al. Chaotic dirac billiard in graphene quantum dots. *Science* **2008**, *320*, 356–358.
2. Shen, J.; Zhu, Y.; Yang, X.; et al. Graphenequantum dots: Emergent nanolights for bioimaging, sensors, catalysis and photovoltaic devices. *Chem. Commun.* **2012**, *48*, 3686–3699.
3. Tian, X.T.; Yin, X.B. Carbon dots, unconventional preparation strategies, and applications beyond photoluminescence. *Small* **2019**, *15*, 1901803.
4. Barati, F.; Avatefi, M.; Moghadam, N.B.; et al. A review of graphene quantum dots and their potential biomedical applications. *J. Biomater. Appl.* **2022**, *37*, 1137–1158.
5. Benítez-Martínez, S.; Valcárcel, M. Graphene quantum dots in analytical science. TrAC-Trend. *Anal. Chem.* **2015**, *72*, 93–113.
6. Bressi, V.; Ferlazzo, A.; Iannazzo, D.; et al. Graphene quantum dots by eco-friendly green synthesis for electrochemical sensing: Recent advances and future perspectives. *Nanomaterials* **2021**, *11*, 1120.
7. Cayuela, A.; Soriano, M.L.; Carrillo-Carrión, C.; et al. Semiconductor and carbon-based fluorescent nanodots: The need for consistency. *Chem. Commun.* **2016**, *52*, 1311–1326.
8. Hua, Y.; Li, S.; Cai, Y.; et al. A sensitive and selective electroanalysis strategy for histidine using the wettable well electrodes modified with graphene quantum dot-scaffolded melamine and copper nanocomposite. *Nanoscale* **2019**, *11*, 2126–2130.
9. Punrat, E.; Maksuk, C.; Chuanuwatanakul, S.; et al. Polyaniline/graphene quantum dot-modified screen-printed carbon electrode for the rapid determination of Cr(VI) using stopped-flow analysis coupled with voltammetric technique. *Talanta* **2016**, *150*, 198–205.
10. Hu, T.; Zhang, L.; Wen, W.; et al. Enzyme catalytic amplification of miRNA-155 detection with graphene quantum dot-based electrochemical biosensor. *Biosens. Bioelectron.* **2016**, *77*, 451–456.
11. Xu, Q.; Yuan, H.; Dong, X.; et al. Dual nanoenzyme modified microelectrode based on carbon fiber coated with AuPd alloy nanoparticles decorated graphene quantum dots assembly for electrochemical detection in clinic cancer samples. *Biosens. Bioelectron.* **2018**, *107*, 153–162.
12. Dan, X.; Ruiyi, L.; Zaijun, L.; et al. Facile strategy for synthesis of silver-graphene hybrid with controllable size and excellent dispersion for ultrasensitive electrochemical detection of acetamiprid. *Appl. Surf. Sci.* **2020**, *512*, 145628.
13. Esmaeili, M.; Ahour, F.; Keshipour, S. Sensitive and selective determination of trace amounts of mercury ions using a dimercaprol functionalized graphene quantum dot modified glassy carbon electrode. *Nanoscale* **2021**, *13*, 11403–11413.
14. Bhatnagar, D.; Kaur, I.; Kumar, A. Ultrasensitive cardiac troponin I antibody based nanohybrid sensor for rapid detection of human heart attack. *Int. J. Biol. Macromol.* **2017**, *95*, 505–510.
15. Ganganboina, A.B.; Dega, N.K.; Tran, H.L.; et al. Application of sulfur-doped graphene quantum dots@gold-carbon nanosphere for electrical pulse-induced impedimetric detection of glioma cells. *Biosens. Bioelectron.* **2021**, *181*, 113151.
16. Wang, X.; Chen, L.; Su, X.; et al. Electrochemical immunosensor with graphene quantum dots and apoferritin-encapsulated Cu nanoparticles double-assisted signal amplification for detection of avian leukosis virus subgroup. *J. Biosens. Bioelectron.* **2013**, *47*, 171–177.
17. Khonsari, Y.N.; Sun, S. A novel label free electrochemiluminescent aptasensor for the detection of lysozyme. *Mater. Sci. Eng. C* **2019**, *96*, 146–152.
18. Nie, G.; Wang, Y.; Tang, Y.; et al. A graphene quantum dots based electrochemiluminescence immunosensor for carcinoembryonic antigen detection using poly(5-formylindole)/reduced graphene oxide nanocomposite. *Biosens. Bioelectron.* **2018**, *101*, 123–128.
19. Long, Y.-M.; Bao, L.; Zhao, J.-Y.; et al. Revealing carbon nanodots as coreactants of the anodic electrochemiluminescence of $Ru(bpy)_3^{2+}$. *Anal. Chem.* **2014**, *86*, 7224–7228.
20. Ahmed, S.R.; Mogus, J.; Chand, R.; et al. Optoelectronic fowl adenovirus detection based on local electric field enhancement on graphene quantum dots and gold nanobundle hybrid. *Biosens. Bioelectron.* **2018**, *103*, 45–53.
21. Pang, X.; Bian, H.; Wang, W.; et al. A bio-chemical application of N-GQDs and g-$C_3N_4$ QDs sensitized $TiO_2$ nanopillars for the quantitative detection of pcDNA3-HBV. *Biosens. Bioelectron.* **2017**, *91*, 456–464.

22. Chung, S.; Revia, R.A.; Zhang, M. Graphene quantum dots and their applications in bioimaging, biosensing, and therapy. *Adv. Mater.* **2021**, *33*, 1904362.
23. Rassheed, P.A.; Ankitha, M.; Pillai, V.K.; et al. Graphene quantum dots for biosensing and bioimaging. *RSC Adv.* **2024**, *14*, 16001–16023.
24. Kammarchedu, V.; Asgharian, H.; Zhou, K.; et al. Recent advances in graphene-based electroanalytical devices for healthcare applications. *Nanoscale* **2024**, *16*, 12857–12882.
25. Durodola, S.S.; Adekunle, A.S.; Olasunkanmi, L.O.; et al. A review on graphene quantum dots for electrochemical detection of emerging pollutants. *J. Fluoresc.* **2022**, *32*, 2223–2236.
26. Ananthanarayanan, A.; Wang, X.; Routh, P.; et al. Facile synthesis of graphene quantum dots from 3D graphene and their application for $Fe^{3+}$ sensing. *Adv. Funct. Mater*. **2014**, *24*, 3021–3026.
27. Li, Q.; Zhang, S.; Dai, L.; et al. Nitrogen-doped colloidal graphene quantum dots and their size-dependent electrocatalytic activity for the oxygen reduction reaction. *J. Am. Chem. Soc.* **2012**, *134*, 18932–18935.
28. Vázquez-Nakagawa, M.; Rodríguez-Pérez, L.; Martín, N.; et al. Supramolecular assembly of edge functionalized top-down chiral graphene quantum dots. *Angew. Chem. Int. Ed.* **2022**, *61*, e202211365.
29. Zhao, Y.; Wu, X.; Sun, S.; et al. A facile and high-efficient approach to yellow emissive graphene quantum dots from graphene oxide. *Carbon* **2017**, *124*, 342–347.
30. Kalita, H.; Palaparthy, V.S.; Baghini, M.S.; et al. Electrochemical synthesis of graphene quantum dots from graphene oxide at room temperature and its soil moisture sensing properties. *Carbon* **2020**, *165*, 9–17.
31. He, M.; Guo, X.; Huang, J.; et al. Mass production of tunable multicolor graphene quantum dots from an energy resource of coke by a one-step electrochemical exfoliation. *Carbon* **2018**, *140*, 508–520.
32. Zhang, Y.; Li, K.; Ren, S.; et al. Coal-derived graphene quantum dots produced by ultrasonic physical tailoring and their capacity for Cu(II) detection. *ACS Sustain. Chem. Eng.* **2019**, *7*, 9793–9799.
33. Yan, X.; Cui, X.; Li, L.-S. Synthesis of large, stable colloidal graphene quantum dots with tunable size. *J. Am. Chem. Soc.* **2010**, *132*, 5944–5945.
34. Kalita, H.; Mohapatra, J.; Pradhan, L.; et al. Efficient synthesis of rice based graphene quantum dots and their fluorescent properties. *RSC Adv.* **2016**, *6*, 23518–23524.
35. Feng, S.; Pan, J.; Li, C.; et al. Folic acid-conjugated nitrogen-doped graphene quantum dots as a fluorescent diagnostic material for MCF-7 cells. *Nanotechnology* **2020**, *31*, 135701.
36. Ochi, Y.; Otani, A.; Katakami, R.; et al. Open system massive synthesis of narrow-band blue and green fluorescent graphene quantum dots and their application in water sensing. *J. Mater. Chem. C* **2024**, *12*, 6548–6558.
37. Zhu, Y.; Dai, C.; Hao, C.; et al. Purification of nitrogen-doped graphene quantum dots and its application in polymer solar cells. *Colloid. Surface. A* **2022**, *648*, 129401.
38. Rao, Z.; Geng, F.; Zhou, Y.; et al. N-doped graphene quantum dots as a novel highly-efficient matrix for the analysis of perfluoroalkyl sulfonates and other small molecules by MALDI-TOF MS. *Anal. Methods* **2017**, *9*, 2014–2020.
39. Guo, Z.; Cai, B.; Cao, Q.; et al. Facile synthesis of amine-functionalized graphene quantum dots with highly pH-sensitive photoluminescence. *Fuller. Nanotube. Car. N.* **2017**, *25*, 704–709.
40. Martins, E.C.; Santana, E.R.; Spinelli, A. Nitrogen and sulfur co-doped graphene quantum dot-modified electrode for monitoring of multivitamins in energy drinks. *Talanta* **2023**, *252*, 123836.
41. Huang, J.J.; Rong, M.Z.; Zhang, M.Q. Preparation of graphene oxide and polymer-like quantum dots and their one- and two-photon induced fluorescence properties. *Phys. Chem. Chem. Phys.* **2016**, *18*, 4800–4806.
42. Huang, W.; Li, X.; Sun, X.; et al. Photoluminescence of graphene quantum dots enhanced by microwave post-treatment. *Chem. Eng. J.* **2021**, *405*, 126714.
43. Li, R.; Liu, Y.; Li, Z.; et al. Bottom-up fabrication of single-layered nitrogen-doped graphene quantum dots through intermolecular carbonization arrayed in a 2D plane. *Chem. Eur. J.* **2015**, *22*, 272–278.
44. Tang, L.; Ji, R.; Li, X.; et al. Size-dependent structural and optical characteristics of glucose-derived graphene quantum dots. *Part. Part. Syst. Char.* **2013**, *30*, 523–531.
45. Jin, H.; Huang, H.; He, Y.; et al. Graphene quantum dots supported by graphene nanoribbons with ultrahigh electrocatalytic performance for oxygen reduction. *J. Am. Chem. Soc.* **2015**, *137*, 7588–7591.
46. Zhu, J.; Tang, Y.; Wang, G.; et al. Green, rapid, and universal preparation approach of graphene quantum dots under ultraviolet irradiation. *ACS Appl. Mater. Interfaces* **2017**, *9*, 14470–14477.
47. Wang, G.; Guo, Q.; Chen, D.; et al. Facile and highly effective synthesis of controllable lattice sulfur-doped graphene quantum dots via hydrothermal treatment of durian. *ACS Appl. Mater. Interfaces* **2018**, *10*, 5750–5759.
48. Dong, P.; Jiang, B.-P.; Liang, W.-Q.; et al. Synthesis of white-light-emitting graphene quantum dots via a one-step reduction and their interfacial characteristics-dependent luminescence properties. *Inorg. Chem. Front.* **2017**, *4*, 712–718.
49. Su, J.; Zhang, X.; Tong, X.; et al. Preparation of graphene quantum dots with high quantum yield by a facile one-step method and applications for cell imaging. *Mater. Lett.* **2020**, *271*, 127806.

50. Shin, Y.; Park, J.; Hyun, D.; et al. Acid-free and oxone oxidant-assisted solvothermal synthesis of graphene quantum dots using various natural carbon materials as resources. *Nanoscale* **2015**, *7*, 5633–5637.
51. Tetsuka, H.; Asahi, R.; Nagoya, A.; et al. Optically tunable amino-functionalized graphene quantum dots. *Adv. Mater.* **2012**, *24*, 5333–5338.
52. Zhang, A.; Chen, T.; Song, S.; et al. Ultrafast generation of highly crystalline graphene quantum dots from graphite paper via laser writing. *J. Colloid Interface Sci.* **2021**, *594*, 460–465.
53. Kang, S.; Ryu, J.H.; Lee, B.; et al. Laser wavelength modulated pulsed laser ablation for selective and efficient production of graphene quantum dots. *RSC Adv.* **2019**, *9*, 13658–13663.
54. Li, L.; Wu, G.; Yang, G.; et al. Focusing on luminescent graphenequantum dots: Current status and future perspectives. *Nanoscale* **2013**, *5*, 4015–4039.
55. Bartolomei, B.; Bogo, A.; Amato, F.; et al. Nuclear Magnetic resonance reveals molecular species in carbon nanodot samples disclosing flaws. *Angew. Chem. Int. Ed.* **2022**, *61*, e202200038.
56. Bartolomei, B.; Prato, M. The importance of the purification step and the characterization of the products in the synthesis of carbon nanodots. *Small* **2023**, *19*, 2206714.
57. Ullal, N.; Mehta, R.; Sunil, D. Separation and purification of fluorescent carbon dots—an unmet challenge. *Analyst* **2024**, *149*, 1680–1700.
58. Jiang, Q.-G.; Cao, C.; Lin, T.-C.; et al. Strong and tough glass with self-dispersed nanoparticles via solidification. *Adv. Mater.* **2019**, *31*, 1901803.
59. Tian, P.; Tang, L.; Teng, K.S.; et al. Graphene quantum dots from chemistry to applications. *Mater. Today Chem.* **2018**, *10*, 221–258.
60. Zhu, S.; Zhang, J.; Tang, S.; et al. Surface chemistry routes to modulate the photoluminescence of graphene quantum dots: From fluorescence mechanism to up-conversion bioimaging applications. *Adv. Funct. Mater.* **2012**, *22*, 4732–4740.
61. Chowdhury, A.D.; Takemura, K.; Li, T.-C.; et al. Electrical pulse-induced electrochemical biosensor for hepatitis E virus detection. *Nat. Commun.* **2019**, *10*, 3737.
62. Dong, Y.; Dai, R.; Dong, T.; et al. Photoluminescence, chemiluminescence and anodic electrochemiluminescence of hydrazide-modified graphene quantum dots. *Nanoscale* **2014**, *6*, 11240–11245.
63. Mirzaie, A.; Hasanzadeh, M.; Jouyban, A. Cross-linked chitosan/thiolated graphene quantum dots as a biocompatible polysaccharide towards aptamer immobilization. *Int. J. Biol. Macromol.* **2019**, *123*, 1091–1105.
64. Dong, Y.; Chen, C.; Zheng, X.; et al. One-step and high yield simultaneous preparation of single- and multi-layer graphenequantum dots from CX-72 carbon black. *J. Mater. Chem.* **2012**, *22*, 8764–8766.
65. Li, Z.; Bu, F.; Wei, J.; et al. Boosting the energy storage densities of supercapacitors by incorporating N-doped graphene quantum dots into cubic porous carbon. *Nanoscale* **2018**, *10*, 22871–22883.
66. Gómez, L.; Martínez, G.; García, S.; et al. Graphene quantum dots: Synthesis and optical properties. *J. Phys. Chem. C* **2021**, *125*, 7124–7134.
67. Nguyen, V.T.; Lee, C.; Nguyen, M.; et al. Single-particle spectroscopy of graphene quantum dots: Structure and emission mechanisms. *ACS Nano* **2020**, *14*, 2781–2791.
68. Zhang, X.; Li, H.; Zhang, M.; et al. Role of surface oxidation in the optical properties of graphene quantum dots: Implications for sensing and bioimaging. *Appl. Surf. Sci.* **2022**, *566*, 155536.
69. Alafeef, M.; Gani, T.; Yang, X.; et al. Fluorescence mechanism of graphene quantum dots: A review on synthesis, emission pathways, and applications. *Small* **2023**, *19*, 2303937.
70. Qing, Y.; Jiang, Y.; Lin, H.; et al. Boosting the supercapacitor performance of activated carbon by constructing overall conductive networks using graphene quantum dots. *J. Mater. Chem.* **2019**, *7*, 6021–6027.
71. Sun, H.; Zhao, A.; Gao, N.; et al. Deciphering a nanocarbon-based artificial peroxidase: Chemical identification of the catalytically active and substrate-binding sites on graphene quantum dots. *Angew. Chem. Int. Ed.* **2015**, *54*, 7176–7180.
72. Zhou, X.; Tian, Z.; Li, J.; et al. Synergistically enhanced activity of graphene quantum dot/multi-walled carbon nanotube composites as metal-free catalysts for oxygen reduction reaction. *Nanoscale* **2014**, *6*, 2603–2607.
73. Wu, J.; Ma, S.; Sun, J.; et al. A metal-free electrocatalyst for carbon dioxide reduction to multi-carbon hydrocarbons and oxygenates. *Nat. Commun.* **2016**, *7*, 13869.
74. Arumugasamy, S.K.; Govindaraju, S.; Yun, K. Electrochemical sensor for detecting dopamine using graphene quantum dots incorporated with multiwall carbon nanotubes. *Appl. Surf. Sci.* **2020**, *508*, 145294.
75. Baluta, S.; Lesiak, A.; Cabaj, J. Graphene quantum dots-based electrochemical biosensor for catecholamine neurotransmitters detection. *Electroanalysis* **2018**, *30*, 1781–1790.
76. Al-Azmi, A.; Keshipour, S. New bidental sulfur-doped graphene quantum dots modified with gold as a catalyst for hydrogen generation. *J. Colloid Interface Sci.* **2022**, *612*, 701–709.
77. Yue, Z.; Lisdat, F.; Parak, W.J.; et al. Quantum-dot-based photoelectrochemical sensors for chemical and biological detection. *ACS Appl. Mater. Interfaces* **2013**, *5*, 2800–2814.

78. Li, L.-L.; Li, J.; Fei, R.; et al. A facile microwave avenue to electrochemiluminescent two-color graphene quantum dots. *Adv. Funct. Mater.* **2012**, *22*, 2971–2979.
79. Kim, S.; Hwang, S.W.; Kim, M.-K.; et al. Anomalous behaviors of visible luminescence from graphene quantum dots: Interplay between size and shape. *ACS Nano* **2012**, *6*, 8203–8208.
80. Lee, S.H.; Kim, D.Y.; Lee, J.; et al. Synthesis of single-crystalline hexagonal graphene quantum dots from solution chemistry. *Nano Lett.* **2019**, *19*, 5437–5442.
81. Shinde, D.B.; Vishal, V.M.; Kurungot, S.; et al. Electrochemical preparation of nitrogen-doped graphene quantum dots and their size-dependent electrocatalytic activity for oxygen reduction. *Bull. Mater. Sci.* **2015**, *38*, 435–442.
82. Kwon, W.; Kim, Y.-H.; Lee, C.-L.; et al. Electroluminescence from graphene quantum dots prepared by amidative cutting of tattered graphite. *Nano Lett.* **2014**, *14*, 1306–1311.
83. Oh, S.D.; Kim, J.; Lee, D.H.; et al. Structural and optical characteristics of graphene quantum dots size-controlled and well-aligned on a large scale by polystyrene-nanosphere lithography. *J. Phys. D Appl. Phys.* **2016**, *49*, 025308.
84. Yeh, T.-F.; Huang, W.-L.; Chung, C.-J.; et al. Elucidating quantum confinement in graphene oxide dots based on excitation-wavelength-independent photoluminescence. *J. Phys. Chem. Lett.* **2016**, *7*, 2087–2092.
85. Jin, L.; Ki, L.; Xu, F.; et al. The synthesis and application of L-cysteine graphene quantum dots for quantitative analysis of nitrite content in water. *Phys. Scr.* **2024**, *99*, 065124.
86. Tetsuka, H.; Nagoya, A.; Fukusumi, T. Molecularly designed, nitrogen-functionalized graphene quantum dots for optoelectronic devices. *Adv. Mater.* **2016**, *28*, 4632–4638.
87. Deka, M.J.; Dutta, A.; Chowdhury, D. Tuning the wettability and photoluminescence of graphene quantum dots via covalent modification. *New J. Chem.* **2018**, *42*, 355–362.
88. Li, R.; Jia, H.; Li, N.; et al. Electrochemical detection of chlorpyrifos in fruits with gold-histidine functionalized graphene quantum dot-graphene hybrid and target-induced DNA cycle amplification. *Sensor. Actuat. B Chem.* **2022**, *355*, 131314.
89. Chen, L.C.; Teng, C.Y.; Lin, C.Y.; et al. Architecting nitrogen functionalities on graphene oxide photocatalysts for boosting hydrogen production in water decomposition process. *Adv. Energy Mater.* **2016**, *6*, 1600719.
90. Li, F.; Yang, D. Non-metal-heteroatom-doped carbon dots: synthesis and properties. *Chem. Eur. J.* **2018**, *25*, 1165–1176.
91. Budak, E.; Ünlü, C. Boron regulated dual emission in B, N doped graphene quantum dots. *Opt. Mater.* **2021**, *111*, 110577.
92. Guo, Z.; Ni, S.; Wu, H.; et al. Designing nitrogen and phosphorus co-doped graphene quantum dots/g-$C_3N_4$ heterojunction composites to enhance visible and ultraviolet photocatalytic activity. *Appl. Surf. Sci.* **2021**, *548*, 149211.
93. Gong, P.; Wang, J.; Hou, K.; et al. Yang. Small but strong: The influence of fluorine atoms on formation and performance of graphene quantum dots using a gradient F-sacrifice strategy. *Carbon* **2017**, *112*, 63–71.
94. Arab, H.; MohammadNejad, S.; MohammadNejad, P. Se-doped $NH_2$-functionalized graphene quantum dot for single-photon emission at free-space quantum communication wavelength. *Quantum Inf. Process.* **2021**, *20*, 184.
95. Hasan, M.T.; Gonzalez-Rodriguez, R.; Ryan, C.; et al. Photo-and electroluminescence from nitrogen-doped and nitrogen-sulfur codoped graphene quantum dots. *Adv. Funct. Mater.* **2018**, *28*, 1804337.
96. Lima, A.R.S.; Mikhraliieva, A.; Vanoni, C.R.; et al. 2D-network of boron-functionalized *N*-doped graphene quantum dots for electrochemical sensing of dopamine. *Diam. Relat. Mater.* **2024**, *146*, 111259.
97. Cheng, H.; Zhao, Y.; Fan, Y.; et al. Graphene-quantum-dot assembled nanotubes: A new platform for efficient Raman enhancement. *ACS Nano* **2012**, *6*, 2237–2244.
98. Wang, D.; Liang, Y.; Su, Y.; et al. Sensitivity enhancement of cloth-based closed bipolar electrochemiluminescence glucose sensor via electrode decoration with chitosan/multi-walled carbon nanotubes/graphene quantum dots-gold nanoparticles. *Biosens. Bioelectron.* **2019**, *130*, 55–64.
99. Du, F.-P.; Cao, N.-N.; Zhang, Y.-F.; et al. PEDOT:PSS/graphene quantum dots films with enhanced thermoelectric properties via strong interfacial interaction and phase separation. *Sci. Rep.* **2018**, *8*, 6441.
100. Jiang, D.; Yang, C.; Fan, Y.; et al. Ultra-sensitive photoelectrochemical aptamer biosensor for detecting *E. coli* O157:H7 based on nonmetallic plasmonic two-dimensional hydrated defective tungsten oxide nanosheets coupling with nitrogen-doped graphene quantum dots ($dWO_3$•$H_2O$@N-GQDs). *Biosens. Bioelectron.* **2021**, *183*, 113214.
101. Yan, Y.; Liu, Q.; Mao, H.; et al. The immobilization of graphene quantum dots by one-step electrodeposition and its application in peroxydisulfate electrochemiluminescence. *J. Electroanal. Chem.* **2016**, *775*, 1–7.
102. Dong, Y.; Tian, W.; Ren, S.; et al. Graphene quantum dots/L-Cysteine coreactant electrochemiluminescence system and its application in sensing lead(II) ions. *ACS Appl. Mater. Interfaces* **2014**, *6*, 1646–1651.
103. Ou, J.; Tao, Y.; Ma, J.; Kong, Y. Well-dispersed chitosan-graphene quantum dots nanocomposites for electrochemical sensing platform. *J. Electrochem. Soc.* **2015**, *162*, H884–H889.
104. Zhao, Q.; Zhou, L.; Li, X.; et al. Au-nitrogen-doped graphene quantum dot composites as “on-off” nanosensors for sensitive photo-electrochemical detection of caffeic acid. *Nanomaterials* **2020**, *10*, 1972.

105. Monisha, S.; Subhashri, M.; Devi, K.S.S.; et al. Defective graphene-nanomaterials derived from banana-biomass for simultaneous electrochemical detection of xanthine, hypoxanthine, and uric acid: Insights from scanning electrochemical microscopy on edge and basal planes. *Electrochim. Acta* **2024**, *497*, 144515.
106. Arumugasamy, S.K.; Chellasamy, G.; Yun, K.; et al. Bio-quantum dots for electrochemical sensing of cardiac biomarkers of acute myocardial infarction. *J. Ind. Eng. Chem.* **2024**, *129*, 488–498.
107. Li, R.; Wei, M.; Zhou, X.; et al. Self-powered sensing platform for monitoring uric acid in sweat using cobalt nanocrystal-graphene quantum dot-$Ti_3C_2T_X$ monolithic film electrode with excellent supercapacitor and sensing behavior. *Microchim. Acta* **2024**, *191*, 530.
108. Cotchim, S.; Kongkaew, S.; Thavarungkul, P.; et al. An unlabeled electrochemical immunosensor uses poly(thionine) and graphene quantum dot-modified activated marigold flower carbon for early prostate cancer detection. *Biosensors* **2024**, *14*, 589.
109. Zahed, F.M.; Hatamluyi, B.; Bojdi, M.K. A sensitive electrochemical sensor based on graphene quantum dots/hierarchical flower-like gold nanostructures for determination of cytostatic drug flutamide. *Mater. Sci. Eng. B* **2024**, *300*, 117109.
110. Yang, Y.; Yan, Q.; Liu, Q.; et al. An ultrasensitive sandwich-type electrochemical immunosensor based on the signal amplification strategy of echinoidea-shaped Au@Ag-$Cu_2O$ nanoparticles for prostate specific antigen detection. *Biosens. Bioelectron.* **2018**, *99*, 450–457.
111. Prasad, B.B.; Kumar, A.; Singh, R. Synthesis of novel monomeric graphene quantum dots and corresponding nanocomposite with molecularly imprinted polymer for electrochemical detection of an anticancerous ifosfamide drug. *Biosens. Bioelectron.* **2017**, *94*, 1–9.
112. Gu, S.; Hsieh, C.-T.; Mallick, B.C.; et al. Non-enzymatic electrochemical detection of hydrogen peroxide on highly amidized graphene quantum dot electrodes. *Appl. Surf. Sci.* **2020**, *528*, 146936.
113. Ma, C.; Cao, Y.; Gou, X.; et al. Recent progress in electrochemiluminescence sensing and imaging. *Anal. Chem.* **2019**, *92*, 431–454.
114. Fan, X.; Wang, S.; Liu, H.; et al. A sensitive electrochemiluminescence biosensor for assay of cancer biomarker (MMP-2) based on NGQDs-Ru@$SiO_2$ luminophore. *Talanta* **2022**, *236*, 122830.
115. Bae, G.; Cho, H.; Hong, B.H. A review on synthesis, properties, and biomedical applications of graphene quantum dots (GQDs). *Nanotechnology* **2024**, *35*, 372001.
116. Huang, Y.; Hu, X.; Zhang, W.; et al. Multiwalled carbon nanorings found in raw single-walled carbon nanotubes and applied for electrochemiluminescent immunoassay. *ACS Sens.* **2025**, *10*, 4589–4599.
117. Zhi, S.; Zhu, Z.; Li, Y.; et al. Electrochemiluminescence detection of catechol and tryptophol using nitrogen, sulfur co-doped graphene quantum dots based on a paper-based sensor. *Microchem. J.* **2024**, *200*, 110408.
118. Ma, L.; Kang, L.; Sun, Y.; et al. Nitrogen-doped graphene quantum dots as electrochemiluminescence-emitting species for sensitive detection of KRAS G12C mutation via PET-RAFT. *Chem. Eur. J.* **2023**, *29*, e202301602.
119. Zhu, Z.; Li, R.; Li, Y.; et al. Paper-based electrodes with nitrogen-doped graphene quantum dots for detection of copper ions via electrochemiluminescence. *Mater. Chem. Phys.* **2023**, *296*, 127300.
120. Liu, M.; Jiang, R.; Zheng, M.; et al. A sensitive ratiometric biosensor for determination cardiac troponin I of myocardial infarction markers based on N, Zn-GQDs. *Talanta* **2022**, *249*, 123577.
121. Wang, B.; Wang, C.; Li, Y.; et al. Electrochemiluminescence biosensor for cardiac troponin I with signal amplification based on a $MoS_2$@$Cu_2O$-Ag-modified electrode and Ce:ZnO-NGQDs. *Analyst* **2022**, *147*, 4768–4776.
122. Liang, X.; Zhang, W.; Zhang, M.; et al. Facile synthesis of nitrogen-doped graphene quantum dots as nanocarbon emitters for sensitive detection of catechol. *RSC Adv.* **2022**, *12*, 25778–25785.
123. Wu, Z.; Dai, C.; Wang, Y.; et al. A novel sensor for visual and selective detection of $Hg^{2+}$ based on functionalized doped quantum dots. *Anal. Methods* **2022**, *14*, 2368–2375.
124. Yuan, R.; Liu, Q.; Hong, H.; et al. Wang. Enhanced cathodic electrochemiluminescent microcystin-LR aptasensor based on surface plasmon resonance of Bi nanoparticles. *J. Hazard. Mater.* **2022**, *434*, 128877.
125. Sun, Y.; Huang, C.; Sun, X.; et al. Electrochemiluminescence biosensor based on molybdenum disulfide-graphene quantum dots nanocomposites and DNA walker signal amplification for DNA detection. *Microchim. Acta* **2021**, *188*, 353.
126. Zheng, Y.; Lin, J.; Xie, L.; et al. One-step preparation of nitrogen-doped graphene quantum dots with anodic electrochemiluminescence for sensitive detection of hydrogen peroxide and glucose. *Front. Chem.* **2021**, *9*, 688358.
127. Liu, P.; Meng, H.; Han, Q.; et al. Determination of ascorbic acid using electrochemiluminescence sensor based on nitrogen and sulfur doping graphene quantum dots with luminol as internal standard. *Microchim. Acta* **2021**, *188*, 120.
128. Li, L.; Chen, B.; Luo, L.; et al. Sensitive and selective detection of $Hg^{2+}$ in tap and canal water via self-enhanced ECL aptasensor based on $NH_2$-Ru@$SiO_2$-NGQDs. *Talanta* **2021**, *222*, 121579.

129. Hou, X.; Suo, Z.; Hu, Z.; et al. Label-free tri-luminophores electrochemiluminescence sensor for microRNAs detection based on three-way DNA junction structure. *J. Electroanal. Chem.* **2021**, *880*, 114935.
130. Jiao, M.; Fan, X.; Wang, Z.; et al. Electrochemiluminescence resonance energy transfer system based on ox-MWCNTs-IGQDs and PdAg nanosheets for the detection of 5-fluorouracil in serum. *Microchem. J.* **2022**, *183*, 108066.
131. Hu, L.; Song, C.; Shi, T.; et al. Dual-quenching electrochemiluminescence resonance energy transfer system from IRMOF-3 coreaction accelerator enriched nitrogen-doped GQDs to ZnO@Au for sensitive detection of procalcitonin. *Sensor. Actuat. B Chem.* **2021**, *346*, 130495.
132. Wu, Z.; Liu, S.; Li, Y.; et al. Electrochemiluminescence resonance energy transfer system fabricated by quantum state complexes for cardiac troponin I detection. *Sensor. Actuat. B Chem.* **2021**, *336*, 129733.
133. Liu, Y.; Sun, Y.; Yang, M. A double-potential ratiometric electrochemiluminescence platform based on g-$C_3N_4$ nanosheets (g-$C_3N_4$ NSs) and graphene quantum dots for $Cu^{2+}$ detection. *Anal. Methods* **2021**, *13*, 903–909.
134. Guo, L.; Li, L.; Luo, L.; et al. Amplified electrochemiluminescence of $Ru(dcbpy)_3^{2+}$ via coreactant active sites on nitrogen-doped graphene quantum dots. *Talanta* **2025**, *286*, 127554.
135. Li, S.; Peng, J.; Lin, X.; et al. RuSiNPs@ N, S-GQDs as self-enhanced anodic electrochemiluminescent immunobeacons for the highly sensitive quantitation of okadaic acid in shellfish. *Microchim. Acta* **2024**, *191*, 737.
136. Cheng, L.-Y.; Qin, L.-L.; Liu, F.-J.; et al. Electrochemiluminescent (ECL) aptasensor for lysozyme using a graphene quantum dot (GQD)-ruthenium bipyridine-silica nanocomposite. *Anal. Lett.* **2025**, *58*, 1204–1213.
137. Luo, L.; Liu, X.; Bi, X.; et al. Dual-quenching effects of methylene blue on the luminophore and co-reactant: Application for electrochemiluminescent-electrochemical ratiometric zearalenone detection. *Biosens. Bioelectron.* **2023**, *222*, 114991.
138. Wei, J.; Chen, L.; Cai, X.; et al. 2D mesoporous silica-confined $CsPbBr_3$ nanocrystals and N-doped graphene quantum dot: A self-enhanced quaternary composite structures for electrochemiluminescence analysis. *Biosens. Bioelectron.* **2022**, *216*, 114664.
139. Li, L.; Chen, B.; Liu, X.; et al. 'On-off-on' electrochemiluminescent aptasensor for $Hg^{2+}$ based on dual signal amplification enabled by a self-enhanced luminophore and resonance energy transfer. *J. Electroanal. Chem.* **2022**, *907*, 116063.
140. Li, Y.; Liu, D.; Meng, S.; et al. Regulation of $Ru(bpy)_3^{2+}$ electrochemiluminescence based on distance-dependent electron transfer of ferrocene for dual-signal readout detection of aflatoxin B1 with high sensitivity. *Anal. Chem.* **2022**, *94*, 1294–1301.
141. Zhou, Y.; Zhang, C.; Liu, J.; et al. Nanochannel confined graphene quantum dots/platinum nanoparticles boosts electrochemiluminescence of luminal-$O_2$ system for sensitive immunoassay. *Talanta* **2025**, *285*, 127223.
142. Zhang, S.; Jiang, M.; Lai, W.; et al. Quenching study of $Cu_2S$-MPA/NGODs composites in electrochemiluminescence detection by modulating resonance energy transfer and adsorption process. *Bioelectrochemistry* **2024**, *159*, 108729.
143. Zheng, L.; Zhang, H.; Won, M.; et al. Codoping g-$C_3N_4$ with boron and graphene quantum dots: Enhancement of charge transfer for ultrasensitive and selective photoelectrochemical detection of dopamine. *Biosens. Bioelectron.* **2023**, *224*, 115050.
144. Meng, L.; Xiao, K.; Zhang, X.; et al. A novel signal-off photoelectrochemical biosensor for M.SssI MTase activity assay based on GQDs@ZIF-8 polyhedra as signal quencher. *Biosens. Bioelectron.* **2020**, *150*, 111861.
145. Deng, Y.; Yan, W.; Guo, Y.; et al. Highly sensitive and selective photoelectrochemical aptasensing of di-2-ethylhexyl phthalate based on graphene quantum dots decorated $TiO_2$ nanotube arrays. *J. Hazard. Mater.* **2022**, *426*, 128107.
146. Bakhshandeh, F.; Saha, S.; Sakib, S.; et al. $TiO_2$ nanoparticles Co-sensitized with graphene quantum dots and pyrocatechol violet for photoelectrochemical detection of Cr(VI). *J. Electrochem. Soc.* **2022**, *169*, 057520.
147. Liao, D.; Zhi, J.; Wang, Q.; et al. Efficient photoelectrochemical aptasensing of di-2-ethylhexyl phthalate in environmental samples based on N, S co-doped graphene quantum dots/$TiO_2$ nanorods. *Anal. Chim. Acta* **2023**, *1271*, 341477.
148. Chen, Q.; Yuan, C.; He, Z.; et al. A label-free photoelectrochemical sensor of S, N co-doped graphene quantum dot (S, N-GQD)-modified electrode for ultrasensitive detection of bisphenol A. *Microchim. Acta* **2022**, *189*, 208.
149. Wu, Z.; Liang, Z.; He, Z.; et al. A label-free photoelectrochemical sensor based on $Bi_2S_3$@nitrogen doped graphene quantum dots for ascorbic acid determination. *Chem. Res. Chin. Univ.* **2022**, *38*, 1387–1393.
150. Zhang, T.; Gu, Y.; Li, C.; et al. Fabrication of novel electrochemical biosensor based on graphene nanohybrid to detect $H_2O_2$ released from living cells with ultrahigh performance. *ACS Appl. Mater. Interfaces* **2017**, *9*, 37991–37999.
151. Xi, J.; Xie, C.; Zhang, Y.; et al. Pd nanoparticles decorated N-doped graphene quantum dots@N-doped carbon hollow nanospheres with high electrochemical sensing performance in cancer detection. *ACS Appl. Mater. Interfaces* **2016**, *8*, 22563–22573.
152. Ju, J.; Chen, W. *In situ* growth of surfactant-free gold nanoparticles on nitrogen doped graphene quantum dots for electrochemical detection of hydrogen peroxide in biological environments. *Anal. Chem.* **2015**, *87*, 1903–1910.

153. Panda, A.K.; Murugan, K.; Sakthivel, R.; et al. A non-enzymatic, biocompatible electrochemical sensor based on N-doped graphene quantum dot-incorporated $SnS_2$ nanosheets for in situ monitoring of hydrogen peroxide in breast cancer cells. *Colloid. Surface. B* **2023**, *222*, 113033.
154. Zhou, C.; Chen, Y.; You, X.; et al. An electrochemiluminescent biosensor based on interactions between a graphene quantum dot-sulfite co-reactant system and hydrogen peroxide. *ChemElectroChem* **2017**, *4*, 1783–1789.
155. Tian, K.; Li, D.; Tang, T.; et al. A novel electrochemiluminescence resonance energy transfer system of luminol-graphene quantum dot composite and its application in $H_2O_2$ detection. *Talanta* **2018**, *185*, 446–452.
156. Chang, L.-Y.; Rinawati, M.; Guo, Y.-T.; et al. Nitrogen-Doped graphene quantum dots incorporated into MOF-derived NiCo layered double hydroxides for nonenzymatic lactate detection in noninvasive biosensors. *ACS Appl. Nano Mater.* **2024**, *7*, 14431–14442.
157. Zhang, H.; Qu, H.; Cui, J.; et al. A simple electrochemical immunosensor based on a chitosan/reduced graphene oxide nanocomposite for sensitive detection of biomarkers of malignant melanoma. *RSC Adv.* **2022**, *12*, 25844–25851.
158. Sapkota, B.; Benabbas, A.; Lin, H.G.; et al. Peptide-decorated tunable-fluorescence graphene quantum dots. *ACS Appl. Mater. Interface*s **2017**, *9*, 9378–9387.